NTNU – Trondheim
Norwegian University of
Science and Technology

Modulation of turbulent channel flow laden with contaminated microbubbles

Majed A. Osama El-Majzoub
Det Malla

Master of Energy and Environmental Engineering
Submission date: June 2013
Supervisor: Helge Ingolf Andersson, EPT
Co-supervisor: Dr. Mustafa Barri, EPT

Norwegian University of Science and Technology
Department of Energy and Process Engineering

NTNU

Norwegian University
of Science and Technology

Department of Energy
and Process egineering

EPT-M-2013-81

MASTER THESIS

for

Stud.techn Majed Det. Malla

Spring 2013

Modulation of turbulent channel flow laden with contaminated microbubbles

Modulering av turbulent strømning i kanal med mikrobobler

Background and objective

The dispersion of microbubbles in turbulent flow has relevance in a number of engineering and environmental applications ranging from bubble columns, gas–liquid reactors, fluidized beds to the transfer mechanisms which couple ocean and atmosphere. In all these applications, the presence of microbubbles, which reportedly are non-uniformly distributed, may significantly change transfer rates. The overall liquid–bubble interface controls gas–liquid transfer, but complex bubble motions also have an influence on overall heat, momentum and mass transfer, playing a crucial role in many industrial and environmental processes.

In this work the dynamic of microbubbles in a vertical turbulent channel flow will be studied numerically by means of Direct Numerical Simulations (DNS's). The microbubbles tracked using point-force lagrangian interpolation scheme with inclusion of the following forces: buoyancy, drag, lift and flow acceleration force.

The following tasks are to be considered:

1- Literature review on the simulation of particle dispersion flow, with focus on
   a) Forces acting on a single microbubble, Maxey & Riley 1983
   b) The effect of Reynolds number and the contamination level in the liquid phase on drag force modification of a single microbubble.
   c) Review of available experiments, models, and simulations.
2- Discus the major numerical approaches to simulate bubble flows.
3- Simulate dispersion microbubble flow under different response times using Euler-Lagrange approach.
4- The findings of the simulations are to be analysed and recommendations given for further advancement in the field.

Within 14 days of receiving the written text on the master thesis, the candidate shall submit a research plan for his project to the department.

When the thesis is evaluated, emphasis is put on processing of the results, and that they are presented in tabular and/or graphic form in a clear manner, and that they are analyzed carefully.

The thesis should be formulated as a research report with summary both in English and Norwegian, conclusion, literature references, table of contents etc. During the preparation of the text, the candidate should make an effort to produce a well-structured and easily readable report. In order to ease the evaluation of the thesis, it is important that the cross-references are correct. In the making of the report, strong emphasis should be placed on both a thorough discussion of the results and an orderly presentation.

The candidate is requested to initiate and keep close contact with his/her academic supervisor(s) throughout the working period. The candidate must follow the rules and regulations of NTNU as well as passive directions given by the Department of Energy and Process Engineering.

Risk assessment of the candidate's work shall be carried out according to the department's procedures. The risk assessment must be documented and included as part of the final report. Events related to the candidate's work adversely affecting the health, safety or security, must be documented and included as part of the final report. If the documentation on risk assessment represents a large number of pages, the full version is to be submitted electronically to the supervisor and an excerpt is included in the report.

Pursuant to "Regulations concerning the supplementary provisions to the technology study program/Master of Science" at NTNU §20, the Department reserves the permission to utilize all the results and data for teaching and research purposes as well as in future publications.

The final report is to be submitted digitally in DAIM. An executive summary of the thesis including title, student's name, supervisor's name, year, department name, and NTNU's logo and name, shall be submitted to the department as a separate pdf file. Based on an agreement with the supervisor, the final report and other material and documents may be given to the supervisor in digital format.

☐ Work to be done in lab (Water power lab, Fluids engineering lab, Thermal engineering lab)

☐ Field work

Department of Energy and Process Engineering, 16. January 2013

Olav Bolland
Department Head

Helge Andersson
Academic Supervisor

Research Advisors: Dr. Mustafa Barri

Abstract

Examining the interaction between microbubbles and turbulence in vertical channel flow is done in this thesis. An Eulerian–Lagrangian approach based on pseudo-spectral direct numerical simulation is used. Babbles, due to their small size, are treated as solid spheres subject to gravity, added mass, pressure gradient, Basset, drag and lift forces, and they are momentum coupled with the fluid. A downward channel flow configuration of water at shear Reynolds number $Re_\tau = 360$ and three different bubble diameters are considered and tested ($d = 110\mu m, 220\mu m\ and\ 330\mu m$) where the bubbles are considered to be non-deformable since they are of small Eotvos Eo number and with no-slip condition applies at bubble surface. As some previous studies, this examination confirms different bubbles distribution in the downflow configuration such as preventing bubbles from reaching the near-wall region. Because of the local momentum exchange with the carrier fluid as well as to the bubble distribution differences, significant decrease of both liquid flow rate and wall shear are observed. We discuss and analyze all the observed trends in this simulation.

The Direct Numerical Simulation (DNS) is the mean used to study such a case. The results are compared with Kim et al. (1987) [30], which is considered as a reference to the turbulent simulation. Statistics related to velocity profile, particles profile and turbulence profile are simulated and discussed closely. This will make us try to understand the physics behind the behavior of the effect of microbubbles in a turbulent flow.

Acknowledgement

I would like to express my gratitude to Prof. Helge Andersson who accepted and guided me through this work and showed his understanding through this short period of time.

I am also gratefully thankful to my dear friend and supervisor Dr. Mustafa Barri for his continuous support for the work, from initial advice & contacts in the early stages of conceptual inception and through ongoing advice and encouragement. I deeply appreciate his help, encouragement, support and guidance through the years and especially in this work.

I want to thank my wife for her undivided and unconditional support and interest, without her, I would be unable to complete my thesis.

List of figures

Nomenclature

ρ	Density (Kg/m^3)
i	subscript: axis direction, velocity component
$+$	superscript: wall scaled variable
α	scaling parameter
t	time (s)
$\vec{u}$	velocity vector (m/s)
u	velocity in x-direction (m/s)
v	velocity in y-direction (m/s)
w	velocity in z-direction (m/s)
$\widetilde{\emptyset}$	instantaneous variable
Φ	upper case, time averaged variable
$\emptyset$	lower case, fluctuating variable
p	pressure (N/m^2)
μ	molecular viscosity $(Kg/(m.s))$
μ_t	"molecular" turbulent/eddy viscosity $(Kg/(m.s))$
v	kinematic viscosity (m^2/s)
v_t	turbulent/eddy viscosity (m^2/s)
$\vec{f}$	body force vector (Nm^3/Kg)
k	turbulence kinetic energy (m^2/s^2)
ϵ	dissipation rate (m^2/s^3)
L	characteristic length (m)
η	Kolmogorov length scale (m)
δ_{ij}	Kronecker delta function
τ_{ij}^t	Reynolds stress tensor (m^2/s^2)
Eo	Eotvos number
R_e	Reynolds number
M	Morton number
g	Gravity force (m/s^2)
d	Diameter (m)
σ	interfacial tension

Contents

Chapter 1

The dispersion of microbubbles in turbulent flow has relevance in a number of engineering and environmental applications ranging from bubble columns, gas–liquid reactors, fluidized beds to the transfer mechanisms which couple ocean and atmosphere. In all these applications, the presence of microbubbles, which reportedly are non-uniformly distributed, may significantly change transfer rates. The overall liquid–bubble interface controls gas–liquid transfer, but complex bubble motions also have an influence on overall heat, momentum and mass transfer, playing a crucial role in many industrial and environmental processes.

This thesis presents the study of the dispersion of microbubbles in a turbulent downflow channel with different bubbles' diameter (*d=110µm, 220µm and 330µm*).

1.1 Introduction

The simultaneous flow of more than one phase is known as the Multiphase flow. This kind of flow occurs in many industrial processes such as: Riser reactors, bubble column reactors, fluidized bed reactors, scrubbers, dryers, oil and gas transport, etc.
Initially, simple assumptions were taken into account by Lockhart and Martinelli [1] to create simple modeling of the multiphase mixtures.

1. The fluids/materials are flowing in well homogeneous mixes.
2. The fluids/materials are flowing separately.

They claimed that there is a relationship between the pressure loss of one phase and the combine phase's pressure loss as a function of pressure loss of the other phase. Nowadays, a map suggested by Taitle and Duckler that is based on five non-dimensional groups is considered useful. This map is not universal and it can be only applied to certain liquid-gas conditions. Classification of such flow can be categorized according to the state of the different phases or components as shown in Figure 1. 1:

- Gas-solid flows (like powder particles in air as ash plume)
- Liquid-solids flows (like polymers in oil)
- Gas-liquid flows (like bubbles in water)
- Solid-solid flows (like sand and grain)
- Liquid-liquid flows (like oil and water)

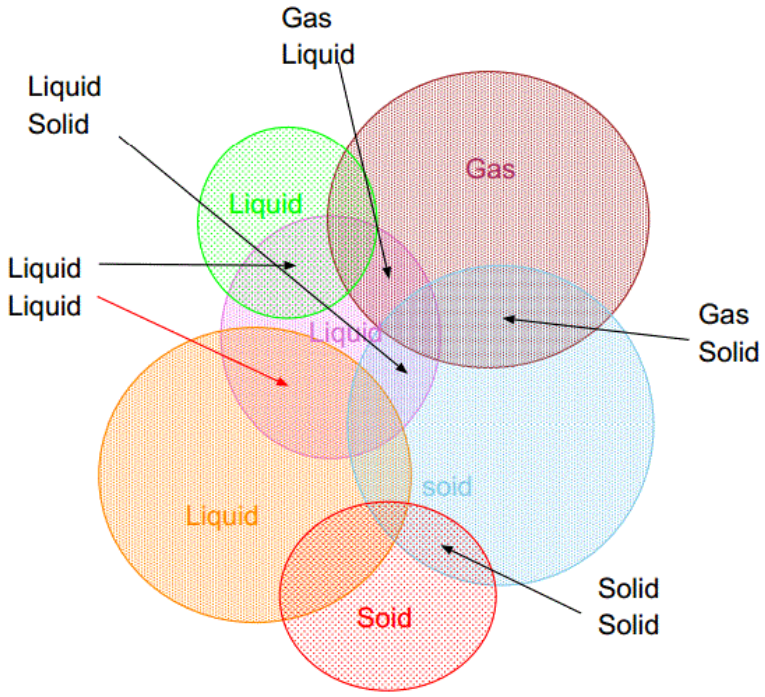

Figure 1. 1

Fields of multiphase flows.

1.2 Classifications of Flow Regimes

The liquid-liquid and the gas-liquid flows will be given special attention here due to the wide use of such categories. There are mainly two possibilities for the two different materials to flow. They can flow in the same direction or in the opposite one, and these two ways are usually referred to as co-current and counter-current respectively. The co-current is more common while the counter-current flow has a limited length window of possibility in the vertical flow.
There is a main difference between the liquid-liquid flow and the gas-liquid one, which is that gas density is much lighter than the liquid density. For example, there is a variation in the gas flow density while the liquid flow density is considered to be constant. This is why the gas-liquid flow would have several flow regimes in one situation while the liquid-liquid flow would have mainly one flow regime.
Regarding the co-current flow, the two liquids can flow either vertically or horizontally and this is defined by the axis the mixture flows with.

1.2.1 Flow regimes in horizontal pipes.

The fact that multi-phase flow can take many different forms makes it difficult and challenging to deal with. These forms are being illustrated in Figure 1. 2 below where 6 different forms can be shown.

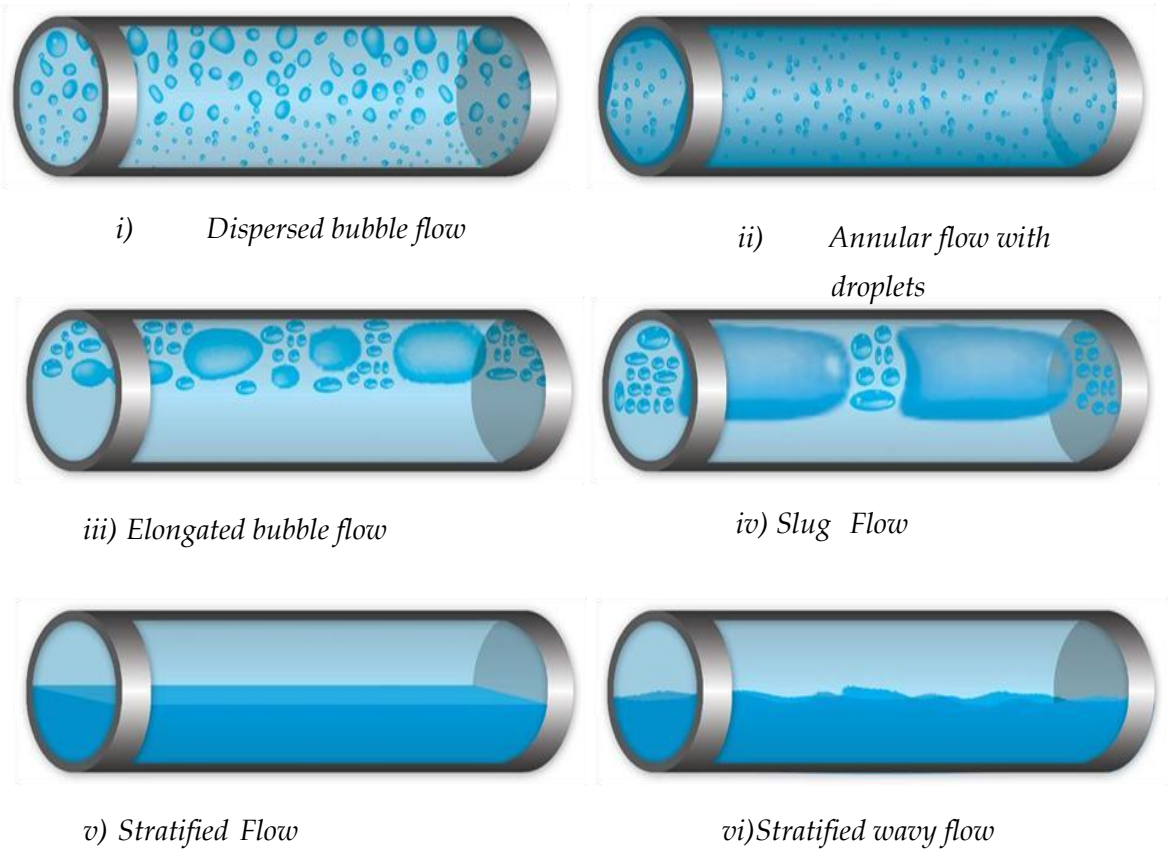

i) Dispersed bubble flow

ii) Annular flow with droplets

iii) Elongated bubble flow

iv) Slug Flow

v) Stratified Flow

vi)Stratified wavy flow

Figure 1. 2

Gas-liquid flow regimes in horizontal pipes.

i) Dispersed Bubble Flow: When both the liquid superficial velocity and the gas superficial velocity are of high values as shown in Figure 1. 3, the regime of the flow would be called dispersed bubble flow.
ii) Annular Flow: When the superficial liquid velocity is intermediate while the gas velocity is high. This indicates that the continuous phase is mainly on the wall and the other phase is positioned in the center of the pipe. It can be defined as “ring-like”.
iii) Elongated Bubble Flow: When both the superficial liquid and gas velocities are in an average range, the elongated bubble flow can be formed. This happens when liquid flow rate is high enough to break up the gas into bubbles but not high enough to cause them to be dispersed.
iv) Slug Flow: This is characterized by the presence of liquid rich slugs that span the pipe diameter. Slugs cause high pressure and liquid flow rate fluctuations.
v) Stratified Flow: When both the liquid and gas (or other liquid) flows are laminar and separated by a clear interface.
vi) Stratified Wavy Flow: This flow is mainly as the Stratified but with increasing the superficial gas velocity which makes the balance between the two phases unequal and causes the disturbance of the interface causing waves.

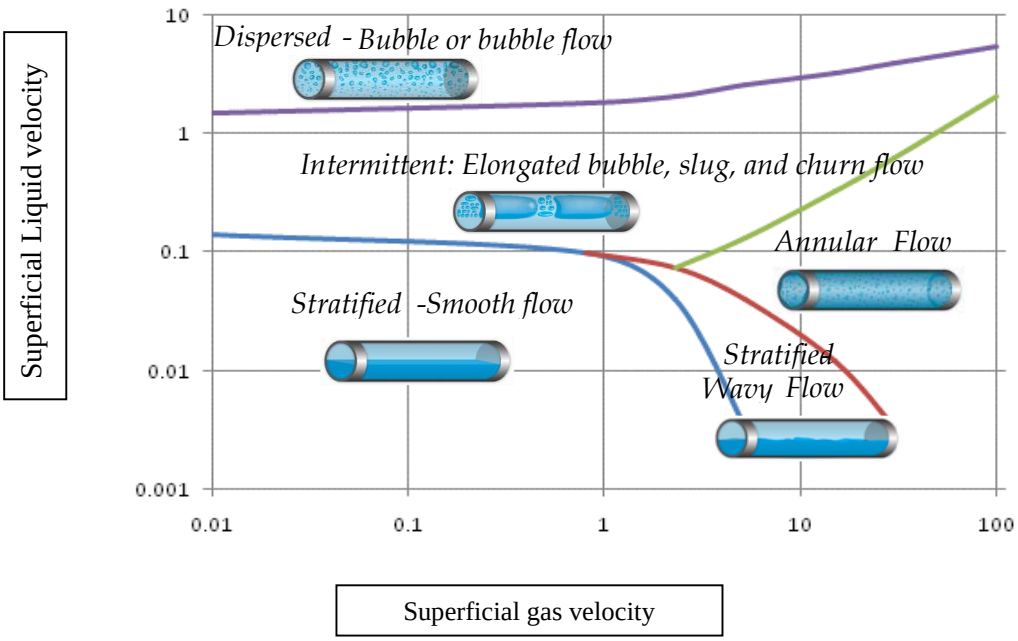

Figure 1. 3

Flow regime map for a horizontal pipe.[2]

1.2.2 Flow Regimes in Vertical Pipes.

The vertical flow gets its definition depending on the flow direction compared to Gravity, Either downflow that means that the flow is moving in the same direction as the gravity or upflow where the flow moves against gravity as shown in Figure 1. 4. The difference between these two kinds of vertical flows is mainly the buoyancy force, which is acting in two different directions. The gas, which is lighter than the liquid, has a buoyancy that acts as an extra force making the flow moves faster in the case of Upflow. In the case of downflow, this buoyancy acts on the opposite direction making the flow slower.

Figure 1. 4

Illustration of the Upflow and Downflow.

The vertical flow regimes are mainly similar to those in horizontal pipes but without the possibility of having stratified flow, since there will not be a lower side of the pipe nor an upper one that the density of the fluid would prefer. Determining what kind of regime flow is crucial for the dynamics of the simulation that is needed. Figure 1. 5 shows the vertical regimes where the Upflow is the case.

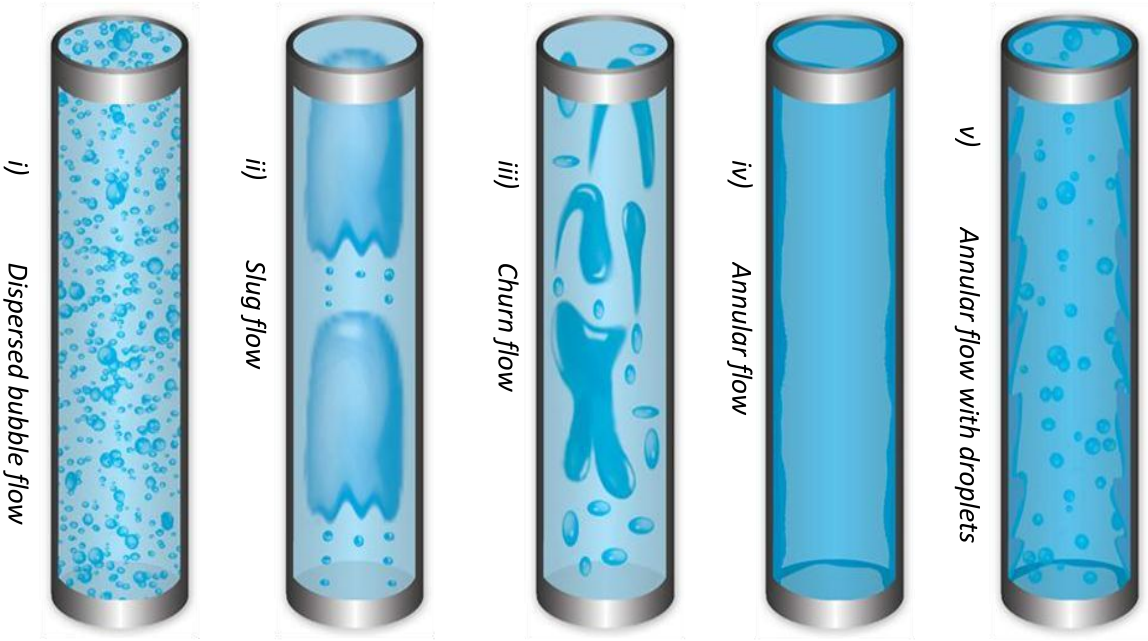

Figure 1. 5

Vertical flow of Upflow regimes of gas and liquid.

The vertical flow starts as bubbly where the lighter liquid flow rate increases. As this flow rate increases, the number of bubbles increases as well until the bubbles start to collide where they create a large bubble in the flow known as slug flow or plug flow. As the lighter liquid flow rate continues to increase, the slug size will increase as more bubbles collide to create a super slug also known as elongated bubble flow as shown in the figure above, Figure 1. *5*. The more turbulent the flow is and as several super slug or churn flow appears, the less stable the flow becomes as it is the case with the annular flow. Further increase of super slug will end by transforming the outer liquid layer into bubbles in the inner liquid.

1.3 Dispersed multiphase flow

In this study, the dispersed flow case will be the main case since the study of micro-bubbles in a turbulent flow is to be determined.
Bubbly flows are important in a wide variety of areas such as environmental phenomena, biomedical field, chemical processes to industrial applications. The presence of micro-bubbles that are non-uniformly distributed in all these applications may change the transfer rate significantly. Because of the their influence, bubbly flows have been analyzed and many studies are available, but the complete understanding of the dynamics of the bubbly flows remains to be a challenging task because of the various factors affecting the bubbles and the surrounding fluid.
In addition to bubbly flow, particles suspended in gas or liquid flow and the dispersion of droplets in a stream of gas are examples of dispersed multiphase flows. These kinds of flows are characterized by a dispersed phase distributed within a carrier phase in the form of droplets, particles, or bubbles.

It is very well known that turbulence and multiphase flow are the two most challenging topics in fluid mechanics especially when they are combined. The nature of the carrier phase turbulence is complicated by the random distribution of the dispersed phase. The numerical simulations of turbulent multiphase flows is much more difficult than those of the single-phase ones due to the presence of the dispersed phase. The insight provided by the computational investigations using Eulerial-Eulerian and Eulerian-Lagrangian techniques were very valuable. An important aspect of the two-phase flow research is the turbulent modulation that has a contribution by several mechanisms such as:

a. Enhanced dissipation due to the presence of particles
b. Transfer of kinetic energy from the particle to the fluid
c. Formation of wakes and vortex shedding behind the particles.

The relative importance of these mechanisms depends on parameters such as the particle-to-turbulence length-scale ratio, particle Reynolds number, and particle-to-fluid density ratio.

Fortunately, the study of bubbly flow has been given a good deal of academic attention in the last three decades. It is of great importance to understand the turbulence modulation of bubbles since it directly controls the heat transfer and the mixing efficiency of bubbly flows and the drag reduction rate by bubbles.

Researchers have already obtained important conclusions by performing studies on turbulent modulation by bubbles. In 1990, Akimi Serizawa and Isao Kataoka summarized three kinds of turbulence suppression mechanisms [3]. Kato et al. reached that the influence of bubble to the liquid turbulence is the same as the solid particle influencing the gas turbulence, where large bubbles increase the liquid phase turbulence and small bubbles reduce the liquid turbulence [4].

Molin et al. [5] and So et al. [6] presented that the bubble size is responsible to the lift force magnitude and direction. Kawamura and Kodama [7] presented that the velocity fluctuations can be influenced by the bubble in two ways where one is called “pseudo-turbulence” and the other is “liquid-phase turbulence modulated by bubbles”. Mazzitelli et al. [8] pointed out that microbubbles accumulating in Downflows locally transfer momentum upwards which is the reason why the increase in microbubbles reduces the vertical velocity fluctuation intensity and the turbulent kinetic energy as well. Ferrante and Elghobashi [9] argued that microbubbles in a spatially developing turbulent boundary layer push the developing streamwise vortices away from the wall, leading to less dissipation in the boundary layer. Tryggvason and Lu [10] pointed out that the bubble deformation is of an important influence on the liquid turbulence.

With all these researches on the turbulence modulation by bubbles, still the turbulence modulation mechanism is not clear yet. This leads to the reason why and how this study was made.

Chapter 2

2.1 Particulate turbulent flow

It is very important to explain the physics behind the particles so it is possible to simulate numerically in order to reach the goal aimed for. However, the physics of bubbles observed in bubbly flows is very complex in addition to the surface deformation and breakup, coalescence and collisions with other bubbles and bubble growth and collapse. First, it is important to mention that bubbles flowing in a liquid are not spherical by default, the shape of the drops or bubbles vary due to buoyancy for different physical parameters. Clift et al. [11] classified freely moving bubbles and drops under the influence of gravity as:

1) *Spherical*: The drops and bubbles are considered to be spherical if interfacial and viscous forces are dominating over inertial forces.
2) *Ellipsoidal*: The drops and bubbles are considered ellipsoidal if they are oblate with a convex surface.
3) *Spherical cap or ellipsoidal cap*: The larger drops or bubbles that tend to be flat, dimpled or skirted at the rear end fall under the category of spherical or ellipsoidal cap.

As illustrated by Clift et al, the different shapes of bubbles and drops can be characterized by three dimensionless numbers: Eotvos number, Morton number and Reynolds number and are defined as:

$$Eo = g\Delta\rho d_e^2/\sigma \tag{1}$$

$$M = g\mu_c^4\Delta\rho/\rho_c^2\sigma^3 \tag{2}$$

$$R_e = \rho_c d_e U/\mu_c \tag{3}$$

Where g is acceleration due gravity, $\Delta\rho$ is the density difference between the continuous phase and the dispersed phase, ρ_c is density of the continuous phase, μ_c is viscosity of the continuous phase, σ is interfacial tension between the two phases and d_e is diameter of the volume-equivalent sphere.

These dimensionless numbers have an effect of the shape of bubbles moving through the liquid because of the gravity, and this effect is very well represented in Figure 2. 1 where the Reynolds number is plotted against the Eotvos number for different values of Morton number.

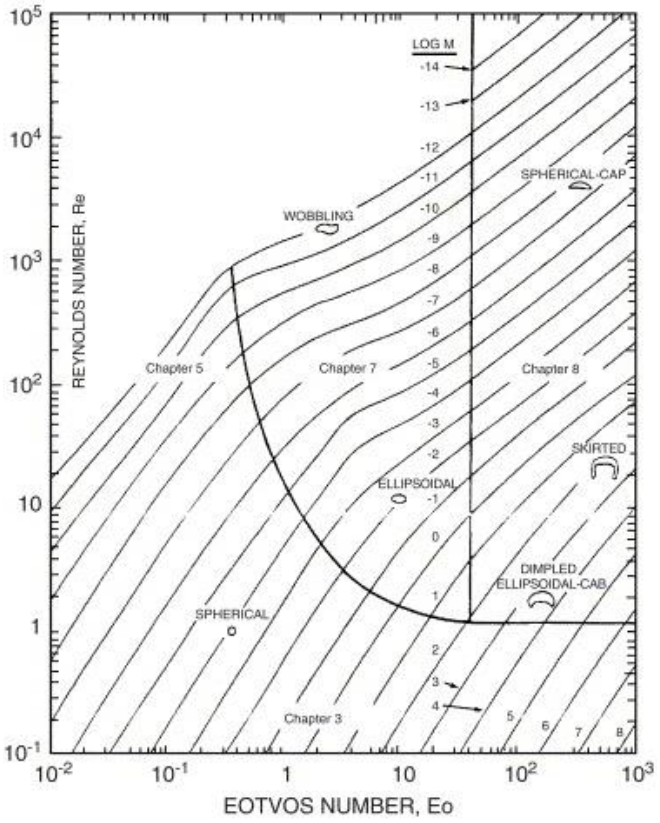

Figure 2. 1

A plot of Reynolds number against Eotvos number for different Morton number is represented along with corresponding shapes of the droplet. Clift et al.

As illustrated above, the bubbles are spherical only if the Eotvos number is of a high value while the Reynolds number is of a low one, or if the Reynolds number is of a high value while the Eotvos number value is low or both Reynolds and Eotvos values are low. Otherwise, the bubbles will have other shapes like ellipsoidal-Cab or wobbling.

Basset [12], Boussinesq [13] and Oseen [14] did the examination of the motion of a rigid sphere settling out under gravity in a fluid at rest earlier in the last century. The motion of the sphere would produce a disturbed flow, which is assumed to be at low Reynolds number that the fluid force on the sphere could be calculated from the results of unsteady Stokes flow. Later, Tchen [15] further examined this work and extended it to a sphere settling under gravity in an unsteady uniform flow at first then in an unsteady non-uniform flow, with a view to application to turbulent flow. Never the less, several errors were detected in Tchen's work and were pointed out by Corrsin and Lumley [16], and they emphasized the role of the pressure gradient of the basic flow to the net fluid force on the particle.

The equation presented by Corrsin and Lumley was still not consistent in that the effects of pressure gradient of the undisturbed flow have been singled out over the effects of viscous shear stress when both effects may well be comparable. This was noted by Buevich [17], who changed the mass of fluid displaced by the sphere term m_F. The same did Riley [18], but instead of using the time derivative following the moving sphere, Riley used the time derivative following the fluid element.

Later, M. R. Maxey [19] gave a rational derivation for the equation of motion of a small sphere with relative motion of low Reynolds number. His final form of the equation of particle motion

after inversion of the transforms presented that it is most likely to neglect the Basset term in the equation. This conclusion is considered to be of great importance due to the numerical complexity of this term.

In general, the forces acting on a particle in a continuous flow (Lagrangian Point Particle Method of Two Phase Flow) are presented as:

$$m_p \frac{d\vec{v}}{dt} = \sum \vec{F} = \vec{F}_B + \vec{F}_D + \vec{F}_L + \vec{F}_F + \vec{F}_{AM} + \vec{F}_{De} + \vec{F}_{BA} \quad (4)$$

Where:

- $\vec{F}_B$ is the Buoyancy Force.
- $\vec{F}_D$ is the Drag Force.
- $\vec{F}_F$ is the Pressure Gradient Force.
- $\vec{F}_L$ is the Lift Force.
- $\vec{F}_{AM}$ is the Added Mass Force.
- $\vec{F}_{BA}$ is the time history Besset Force.
- $\vec{F}_{De}$ is the particle Deformation Force.

$$\vec{F}_B = \left(m_p - m_f\right)\vec{g} \quad (5)$$

$$\vec{F}_D = \frac{1}{2}\rho_f A_p C_D \left|\vec{u} - \vec{v}\right| (\vec{u} - \vec{v}) \quad (6)$$

$$\vec{F}_F = m_f \frac{D\vec{u}}{Dt} \quad (7)$$

$$\vec{F}_L = m_f C_L (\vec{u} - \vec{v}) \times \vec{w} \quad (8)$$

$$\vec{F}_{AM} = \frac{d}{dt}\left(\rho_f C_\mu V_p (\vec{u} - \vec{v})\right) = m_f C_\mu \left(\frac{D\vec{u}}{Dt} - \frac{d\vec{u}}{dt}\right) + \frac{3 m_f C_\mu}{R_p} (\vec{u} - \vec{v}) \frac{dR_p}{dt} \quad (9)$$

$$\vec{F}_{BA} = 6\pi\mu R_p^2 \int_0^t \frac{1}{[\pi\nu(t-\tau)]^{\frac{1}{2}}} \frac{d}{d\tau} (\vec{u} - \vec{v}) d\tau \quad (10)$$

$$\vec{F}_{De} = 4\pi\rho_f R_p^2 C_\mu (\vec{u} - \vec{v}) \frac{dR_p}{dt} \quad (11)$$

m_p is the particle mass, m_f is the mass of fluid displaced by the sphere and the density of the carrier-phase is ρ_f. $\vec{g}$ is the Gravity, $\vec{u}$ is the carrier-phase velocity, $\vec{v}$ is the particle velocity and A_p is the area of a particle with radius R_p. C_D is the coefficient of the bubble drag, $C_L$and C_μ are the lift coefficient and the added mass coefficient respectively. $\mu \; and \; \nu$ are the dynamic viscosity and the kinematic viscosity respectively.

For more clarity, the definition of each term is:

* $A_p = \pi R_p^2, \quad V_p = \frac{3}{4}\pi R_p^3$
* $m_p = \rho_p V_p, \; m_f = \rho_f V_p$
* $\vec{w} = \nabla \times \vec{u}$
* $\frac{D}{Dt} = \frac{\partial}{\partial t} + \vec{u}.\nabla = \frac{\partial}{\partial t} + u_j \frac{\partial}{\partial_{xj}}$ The material derivative
* $\frac{d}{dt} = \frac{\partial}{\partial t} + \vec{v}.\nabla = \frac{\partial}{\partial t} + v_j \frac{\partial}{\partial_{xj}}$ The Lagrangian derivative

So dividing (4) by the mass of the particle, the acceleration equation including the Basset term becomes:

$$\frac{d\vec{v}}{dt} = \left(1 - \frac{\rho_f}{\rho_p}\right)\vec{g} + \frac{1}{\tau_p}(\vec{u} - \vec{v})C_s + \frac{V_f}{V_p}C_L(\vec{u} - \vec{v}) \times \vec{w} + \frac{\rho_f}{\rho_p}\frac{D\vec{u}}{Dt} + \frac{\rho_f}{\rho_p}C_\mu\left(\frac{D\vec{u}}{Dt} - \frac{d\vec{v}}{dt}\right) + \frac{\rho_f}{\rho_p}\frac{3C_\mu}{R_p}(\vec{u} - \vec{v})\frac{dR_p}{dt} + \frac{9\mu}{2\rho_p R_p}\int_0^t \frac{1}{[\pi\nu(t-\tau)]^{1/2}}\frac{d}{d\tau}(\vec{u} - \vec{v})d\tau \quad (12)$$

To modify the Stokesian drag force for larger bubble Reynolds number (Re_p), the non-linear correction coefficient was included as Schiller and Naumann presented [20].

$$Re_p = \frac{2R_p|\vec{u} - \vec{v}|}{\nu} \quad (13)$$

The focus in this work is the bubbles that are considered to behave as small rigid spheres, this hypothesis is valid if the bubble diameter is small enough to satisfy the condition where $Eo < 0.2$ as suggested by Michaelides [21] related to Figure 2. 1. The bubble internal circulation effects are neglected due to the low ratio of bubble density to fluid density. These assumptions justify the coefficients in Eq. (12). In the drag force term, τ_p is the characteristic time of the bubble, defined as:

$$\tau_p = \left(4R_p^2\rho_p\right)/18\nu\rho_f \quad (14)$$

In the lift term, the lift coefficient C_L is a function of bubble Reynolds number and the dimensionless parameter Sr_p defined as:

$$Sr_p = \frac{|(\vec{u} - \vec{v}) \times \vec{w}|2R_p}{|\vec{u} - \vec{v}|^2} \quad (15)$$

C_L is calculated according to Legendre and Magnaudet [22] where it is expressed as:

$$C_L = \left[\left(\frac{6J}{\pi^2\left(Re_p Sr_p\right)^{1/2}}\right)^2 + \left(\frac{1}{2}\frac{Re_p + 16}{Re_p + 29}\right)^2\right]^{1/2} \quad (16)$$

Where

$$J = \frac{2.225}{(1 + 0.2\ \epsilon^{-2})^{3/2}} \tag{17}$$

$$\epsilon = \left(\frac{Sr_p}{Re_p}\right)^{1/2} \tag{18}$$

By using the Schiller and Naumann [23] drag model, the drag coefficient is defined as:

$$C_D = \begin{cases} \left(\frac{24}{Re_p}\right)\left(1 + 0.15Re_p^{0.687}\right) & Re_p < 1000 \\ 0.44 & Re_p > 1000 \end{cases} \tag{19}$$

$$C_s = (1 + 0.15Re_p^{0.687}) \tag{20}$$

By neglecting the Basset Force term and simplifying Eq. (12) by introducing some assumptions as:

$$D = \frac{\rho_p}{\rho_f} \tag{21}$$

$$\beta = \frac{(1 + C_\mu)\rho_f}{\rho_p + \rho_f C_\mu} = \frac{(1 + C_\mu)}{D + C_\mu} \tag{22}$$

Then the acceleration equation becomes:

$$\frac{d\vec{v}}{dt} = (1 - \beta)\vec{g} + \left(1 - \frac{\beta C_\mu}{1+C_\mu}\right)\frac{C_s}{\tau_p}(\vec{u} - \vec{v}) + \frac{\beta}{(1+C_\mu)} C_L(\vec{u} - \vec{v}) \times \vec{w} + \beta\frac{D\vec{u}}{Dt} + \frac{\beta C_\mu}{(1+C_\mu)}\frac{3}{R_p}\frac{dR_p}{dt} \tag{23}$$

With some more assumptions as:

$$\frac{1}{\tau_s} = \frac{\left(1 - \frac{\beta C_\mu}{(1 + C_\mu)}\right)}{\tau_p} = \frac{9v\beta}{2(1 + C_\mu)R_p^2}$$
$$\Rightarrow \tau_s = \frac{2(1 + C_\mu)R_p^2}{9v\beta} = \frac{\tau_p(1 + C_\mu)}{\beta D} \tag{24}$$
$$\tau_p = \frac{2DR_p^2}{9v},\ \frac{C_s}{\tau_p} = \frac{3vC_D Re_p}{16DR_p^2}$$

By using the Rayleigh-Plesset equation [24], where S is the surface tension of the bubble:

$$\rho_f\left[R_p\frac{d^2R_p}{dt^2} + \frac{3}{2}\left(\frac{dR_p}{dt}\right)^2\right] = P_B - P_\infty + \frac{2S}{R_p} + \frac{4\mu}{R_p}\frac{dR_p}{dt} \tag{25}$$

The acceleration equation gets to be as such:

$$\frac{d\vec{v}}{dt} = (1-\beta)\vec{g} + \frac{C_s}{\tau_s}(\vec{u}-\vec{v}) + \frac{\beta}{(1+C_\mu)} C_L(\vec{u}-\vec{v}) \times \vec{w} + \beta\frac{D\vec{u}}{Dt} + \frac{\beta C_\mu}{(1+C_\mu)}\frac{3}{R_p}\frac{dR_p}{dt} \quad (26)$$

Finally, by having a constant value for the added mass coefficient (Batchelor [25]):

$$C_\mu = \frac{1}{2} \quad \text{Then:} \quad \beta = \frac{3}{1+2D}, \ \frac{1}{\tau_s} = \frac{3\nu\beta}{R_p^2} = \frac{3-\beta}{3\tau_p} \quad (27)$$

The acceleration equation gets its final shape as:

$$\frac{d\vec{v}}{dt} = (1-\beta)\vec{g} + \frac{C_s}{\tau_s}(\vec{u}-\vec{v}) + \frac{2}{3}\beta C_L(\vec{u}-\vec{v}) \times \vec{w} + \beta\frac{D\vec{u}}{Dt} + \frac{\beta}{R_p}\frac{dR_p}{dt} \quad (28)$$

Eq. 28 is a general form of the acceleration equation for particles regardless of what type these particles are. By dividing these types of particles into three categories which are; Solid Particles, Microbubbles, and Buoyant Particles. Then Eq. 28 gets to be as such:

- For Solid Particles: $(D \gg 1)$: $\beta = 0$

$$\frac{d\vec{v}}{dt} = \vec{g} + \frac{C_s}{\tau_s}(\vec{u}-\vec{v}) \quad (29)$$

- For Microbubbles: $(D \ll 1)$: $\beta = 3$

$$\frac{d\vec{v}}{dt} = -2\vec{g} + \frac{C_s}{\tau_s}(\vec{u}-\vec{v}) + 2C_L(\vec{u}-\vec{v}) \times \vec{w} + 3\frac{D\vec{u}}{Dt} + \frac{3}{R_p}\frac{dR_p}{dt} \quad (30)$$

- For Buoyant Particles: $(D = 1)$: $\beta = 1$

$$\frac{d\vec{v}}{dt} = \frac{C_s}{\tau_s}(\vec{u}-\vec{v}) + \frac{2}{3}C_L(\vec{u}-\vec{v}) \times \vec{w} + \frac{D\vec{u}}{Dt} + \frac{1}{R_p}\frac{dR_p}{dt} \quad (31)$$

As mentioned before, the case for microbubbles is the focus in this thesis, so Eq. 30 will be adopted.

2.2 Turbulent Flow

Most of fluid flows found in nature and in engineering problems are turbulent. It is extremely difficult to predict the turbulent flow, yet the equations describing the turbulent motions have been known for over a century but still too complex to solve analytically. For many years, only physical experiments were applied on these flows but with the possibility of computational resources that increased recently, it became possible to solve the equations of fluid flow numerically. It became very popular to use computational fluid dynamics (CFD) in industries during the last few decades, mainly through the simplifying approach of turbulence modelling. Even though the CFD is of great importance due to the advantages provided compared with the experiments, still CFD is not a substitute but rather an additional solving tool. CFD results are at best as good as the underlying physics embedded in the code written, and at worst as good as its operator. In order to be validated they need to be compared with experimental data from a similar setup. A skilled operator who can make the correct modelling choices and evaluate the results is therefore essential.

The conservation laws are divided into conservation of mass, conservation of linear momentum (Newton's Second Law of motion) and conservation of energy (First Law of Thermodynamics), where these conservation laws are applied to an infinitesimally small control volume that is small enough to encapsulate a fluid element, but not so small that intermolecular actions are of importance. This is explained by having a small Knudsen number($K_n = \frac{\lambda}{L}$), which is the ratio of the molecular mean free path (λ) and a representative physical length scale (L). Out of these conservation laws and the control volume, the continuity equation, momentum equation and the energy equation are derived. These equations are presented as the following:

$$\frac{\partial \rho}{\partial t} + \frac{\partial \rho u_i}{\partial x_i} = 0 \tag{32}$$

$$\frac{\partial \rho u_i}{\partial t} + \frac{\partial \rho u_i u_j}{\partial x_j} = -\frac{\partial p}{\partial x_i} + \frac{\partial \tau_{ij}}{\partial x_j} + \rho f_i \tag{33}$$

$$\frac{\partial \rho e}{\partial t} + \frac{\partial \rho e u_i}{\partial x_i} = k\frac{\partial^2 T}{\partial x_i^2} - \frac{\partial p u_i}{\partial x_i} + \frac{\partial \tau_{ij} u_i}{\partial x_i} + \rho f_i u_i + \rho \dot{q} \tag{34}$$

These equations are the general equations of fluid dynamics, but we will be dealing with incompressible Newtonian fluid that means zero volumetric deformation and the viscous stresses are proportional to the rate of deformation.

$$\frac{\partial u_i}{\partial x_i} = 0 \tag{35}$$

$$\tau_{ji} = \tau_{ij} = \mu\left(\frac{\partial u_i}{\partial x_j} + \frac{\partial u_j}{\partial x_i}\right) \tag{36}$$

So the final equation is:

$$\rho\left(\frac{\partial u_i}{\partial t} + u_j\frac{\partial u_i}{\partial x_j}\right) = -\frac{\partial p}{\partial x_i} + 2\mu\frac{\partial}{\partial x_j}s_{ij} \tag{37}$$

$$s_{ij} = \frac{1}{2}\left(\frac{\partial u_i}{\partial x_j} + \frac{\partial u_j}{\partial x_i}\right) \tag{38}$$

s_{ij} is the strain rate tensor, τ_{ji} is the Reynolds stress tensor.

2.2.1 Fluctuating turbulent kinetic energy

An equation is needed to represent the turbulent kinetic energy when investigating the dissipation of the turbulent energy. Reynolds decomposition is used to get this equation where the instantaneous flow is presented as a time averaged variable and a fluctuating variable.

$$\widetilde{\emptyset} = \Phi + \emptyset \tag{39}$$

Where Φ is defined by:

$$\Phi \equiv \frac{1}{T}\int_{t_0}^{t_0+T} \widetilde{\emptyset} dt \tag{40}$$

We decompose Eq. (37) by applying (39), then we get:

$$\rho\left(\frac{\partial}{\partial t}(U_i + u_i) + \left(U_j + u_j\right)\frac{\partial}{\partial x_j}(U_i + u_i)\right) = -\frac{\partial}{\partial x_i}(P + p) + 2\mu\frac{\partial}{\partial x_j}\left(S_{ij} + s_{ij}\right) \tag{41}$$

By expanding, we get:

$$\frac{\partial U_i}{\partial t} + \frac{\partial u_i}{\partial t} + U_j\frac{\partial U_i}{\partial x_j} + U_j\frac{\partial u_i}{\partial x_j} + u_j\frac{\partial U_i}{\partial x_j} + u_j\frac{\partial u_i}{\partial x_j} = -\frac{1}{\rho}\frac{\partial}{\partial x_i}(P + p) + 2v\frac{\partial}{\partial x_j}\left(S_{ij} + s_{ij}\right) \tag{42}$$

Multiplying the whole equation by u_i and time average will result in a Reynolds Averaged equation:

$$\overline{u_\iota\frac{\partial U_\iota}{\partial t}} + \overline{u_\iota\frac{\partial u_\iota}{\partial t}} + \overline{u_\iota U_J\frac{\partial U_\iota}{\partial x_J}} + \overline{u_\iota U_J\frac{\partial u_\iota}{\partial x_J}} + \overline{u_\iota u_J\frac{\partial U_\iota}{\partial x_J}} + \overline{u_\iota u_J\frac{\partial u_\iota}{\partial x_J}} = \overline{-\frac{u_\iota}{\rho}\frac{\partial}{\partial x_J}(P + p)} + \overline{2vu_\iota\frac{\partial}{\partial x_J}\left(S_{\iota J} + s_{\iota J}\right)} \tag{43}$$

Where $\overline{U} = U, \bar{u} = 0, \overline{Uu} = \overline{U}\bar{u} = 0\ and\ \overline{uu} \neq 0$. By using these terms in Eq. (43), we get the following terms.

$$\overline{u_\iota\frac{\partial U_\iota}{\partial t}} = \bar{u}_\iota\frac{\partial \overline{U}_\iota}{\partial t} = 0.\frac{\partial U_i}{\partial t} = 0 \tag{44.1}$$

$$\overline{u_\iota\frac{\partial u_\iota}{\partial t}} = \overline{\frac{\partial\frac{1}{2}u_\iota u_\iota}{\partial t}} = \frac{\partial k}{\partial t}, where\ k = \frac{1}{2}\overline{u_\iota u_\iota} \tag{44.2}$$

$$\overline{u_\iota U_J\frac{\partial U_\iota}{\partial x_J}} = 0 \tag{44.3}$$

$$\overline{u_\iota U_J\frac{\partial u_\iota}{\partial x_J}} = U_j\frac{\partial k}{\partial x_j} \tag{44.4}$$

$$\overline{u_\iota u_J \frac{\partial U_\iota}{\partial x_J}} = \overline{u_\iota u_J}\frac{1}{2}\left(\frac{\partial U_i}{\partial x_j} + \frac{\partial U_j}{\partial x_i}\right) = \overline{u_\iota u_J} S_{ij} \tag{44.5}$$

$$\overline{u_\iota u_J \frac{\partial u_\iota}{\partial x_J}} = \frac{\partial}{\partial x_j}\left(\frac{1}{2}\overline{u_\iota u_\iota u_J}\right) \tag{44.6}$$

$$\overline{-\frac{u_\iota}{\rho}\frac{\partial}{\partial x_\iota}(P+p)} = -\frac{\partial}{\partial x_i}(\overline{u_\iota p}) \tag{44.7}$$

$$\overline{2\nu u_\iota \frac{\partial}{\partial x_J}\left(S_{\iota J} + s_{\iota J}\right)} = 2\nu\frac{\partial}{\partial x_j}\left(\overline{u_\iota s_{\iota J}}\right) - 2\nu\overline{s_{\iota J} s_{\iota J}} \tag{44.8}$$

By using (44) into Eq. (43), we get the kinetic energy equation for turbulence fluctuations:

$$\frac{\partial k}{\partial t} + U_j\frac{\partial k}{\partial t} = -\frac{\partial}{\partial x_j}\left[\frac{1}{\rho}\overline{u_J p} + \frac{1}{2}\overline{u_\iota u_\iota u_J} - 2\nu\overline{u_\iota s_{\iota J}}\right] - \overline{u_\iota u_J} S_{ij} - 2\nu\overline{s_{\iota J} s_{\iota J}} \tag{45}$$

This form of equation is not convenient for studying the viscous term, so we introduce some changes into Eq. (44.8) as such:

$$\overline{2\nu u_\iota \frac{\partial}{\partial x_J}\left(S_{\iota J} + s_{\iota J}\right)} = \overline{2\nu u_\iota \frac{\partial}{\partial x_J} s_{\iota J}} = \nu\overline{u_\iota \frac{\partial^2 u_\iota}{\partial x_J^2}} \tag{46}$$

$$\frac{\partial k}{\partial t} + U_j\frac{\partial k}{\partial t} = -\frac{\partial}{\partial x_j}\left[\frac{1}{\rho}\overline{u_J p} + \frac{1}{2}\overline{u_\iota u_\iota u_J}\right] - \overline{u_\iota u_J} S_{ij} + \nu\overline{u_\iota \frac{\partial^2 u_\iota}{\partial x_J^2}} \tag{47}$$

Eq. (47) is a transport equation, which means that the viscous term consists of two different effects, a sink/source effect and a transport one (Corrsin [25]). It behaves as a sink as it describes the rate of dissipation of turbulent energy to heat as well as it describes the rate of transport of turbulent energy by viscous forces, hence:

$$\nu\overline{u_\iota \frac{\partial^2 u_\iota}{\partial x_J^2}} = T - \emptyset \tag{48}$$

$\emptyset$ is the fluctuations of the decomposed and time averaged general dissipation function:

$$\epsilon = \Phi + \emptyset = \nu\overline{\frac{\partial U_\iota}{\partial x_J}\left(\frac{\partial U_\iota}{\partial x_J} + \frac{\partial U_J}{\partial x_\iota}\right)} + \nu\overline{\frac{\partial u_\iota}{\partial x_J}\left(\frac{\partial u_\iota}{\partial x_J} + \frac{\partial u_J}{\partial x_\iota}\right)} \tag{49}$$

So by introducing $\emptyset$ to Eq. (48), we get:

$$\nu\overline{u_\iota \frac{\partial^2 u_\iota}{\partial x_J^2}} = T - \nu\overline{\frac{\partial u_\iota}{\partial x_J}\left(\frac{\partial u_\iota}{\partial x_J} + \frac{\partial u_J}{\partial x_\iota}\right)} \tag{50}$$

By arranging the left hand side, we get:

$$\nu\frac{\partial^2 \frac{1}{2}\overline{u_i^2}}{\partial x_J^2} = \nu\frac{\partial}{\partial x_J}\overline{\left(u_\iota\frac{\partial u_\iota}{\partial x_J}\right)} = \nu\overline{\frac{\partial u_\iota}{\partial x_J}\frac{\partial u_\iota}{\partial x_J}} + \nu\overline{u_\iota\frac{\partial^2 u_\iota}{\partial x_J^2}} \tag{51}$$

$$\overline{\nu u_\iota \frac{\partial^2 u_\iota}{\partial x_j^2}} = \underbrace{\nu \frac{\partial^2 \frac{1}{2}\overline{u_\iota^2}}{\partial x_j^2}}_{\text{Incomplete transport}} - \underbrace{\nu \overline{\frac{\partial u_\iota}{\partial x_j}\frac{\partial u_\iota}{\partial x_j}}}_{\text{Homogeneous dissipation}} \tag{52}$$

The viscous term ends up with two different equations, (Eq. (50 & 52)). T can be solved:

$$\nu \frac{\partial^2 \frac{1}{2}\overline{u_\iota^2}}{\partial x_j^2} - \nu \overline{\frac{\partial u_\iota}{\partial x_j}\frac{\partial u_\iota}{\partial x_j}} = T - \nu \overline{\frac{\partial u_\iota}{\partial x_j}\left(\frac{\partial u_\iota}{\partial x_j} + \frac{\partial u_j}{\partial x_\iota}\right)} \tag{53}$$

$$T = \nu \frac{\partial^2 \frac{1}{2}\overline{u_\iota^2}}{\partial x_j^2} + \nu \overline{\frac{\partial^2 u_\iota u_j}{\partial x_\iota \partial x_j}} \tag{54}$$

We finally get this viscous term:

$$\overline{\nu u_\iota \frac{\partial^2 u_\iota}{\partial x_j^2}} = \underbrace{\nu \left(\frac{\partial^2 k}{\partial x_j^2} + \overline{\frac{\partial^2 u_\iota u_j}{\partial x_j \partial x_j}}\right)}_{\text{Full transport}} - \underbrace{\nu \overline{\frac{\partial u_\iota}{\partial x_j}\left(\frac{\partial u_\iota}{\partial x_j} + \frac{\partial u_j}{\partial x_\iota}\right)}}_{\text{correct transport}} \tag{55}$$

Eq. (55) describes the correct physical behavior of the viscous term in the equation for fluctuating turbulent kinetic energy while Eq. (52) is not correct when discussing inhomogeneous dissipation. Homogeneous turbulence means that the spatial derivatives of all mean turbulence quantities are zero. This can be presented by reducing Eq. (45) to:

$$\frac{\partial k}{\partial t} = -\overline{u_\iota u_j} S_{ij} + \nu \overline{s_{\iota j} s_{\iota j}} \tag{56}$$

In addition, Eq. (57) is reduced to:

$$\frac{\partial k}{\partial t} = -\overline{u_\iota u_j} S_{ij} + \nu u_\iota \overline{\frac{\partial^2 u_\iota}{\partial x_j^2}} \tag{57}$$

The last term in Eq. (57) is reduced due to homogeneous turbulence and becomes as:

$$\overline{\nu u_\iota \frac{\partial^2 u_\iota}{\partial x_j^2}} = -\nu \overline{\frac{\partial u_\iota}{\partial x_j}\frac{\partial u_\iota}{\partial x_j}} \tag{58}$$

By simplification, we get:

$$\epsilon = 2\ \nu \overline{s_{\iota j} s_{\iota j}} = \nu \overline{\frac{\partial u_\iota}{\partial x_j}\left(\frac{\partial u_\iota}{\partial x_j} + \frac{\partial u_j}{\partial x_\iota}\right)} = \nu \overline{\frac{\partial u_\iota}{\partial x_j}\frac{\partial u_\iota}{\partial x_j}} \tag{59}$$

The utilization of this simplification is mainly used in the turbulence models where its transport equation is less complicated than for the full term.

2.2.2 Reynolds stresses

Reynolds stresses' derivation is similar to the derivation of Eq. (45), where the exact transport equations for the transport of the Reynolds stresses, $\rho\tau_{ij}$, may be written as follows [31]:

$$\begin{aligned}
&\frac{\partial}{\partial t}\left(\rho\overline{u_\iota u_j}\right) + \underbrace{\frac{\partial}{\partial x_k}\left(\rho\overline{U}_k\overline{u_\iota u_j}\right)}_{C_{ij}\equiv convection} = \\
&\underbrace{-\frac{\partial}{\partial x_k}\left[\rho\overline{u_\iota u_j u_k} + \overline{p\left(\delta_{kj}u_\iota + \delta_{\iota k}u_j\right)}\right]}_{D_{ij}\equiv Turbulent\ Diffusion} \\
&\underbrace{+\frac{\partial}{\partial x_k}\left[\mu\frac{\partial}{\partial x_k}\left(\overline{u_\iota u_j}\right)\right]}_{D_{L,ij}\equiv Molecular\ Diffusion} \quad \underbrace{-\rho\left(\overline{u_\iota u_k}\frac{\partial\overline{U}_i}{\partial x_k} + \overline{u_j u_k}\frac{\partial\overline{U}_j}{\partial x_k}\right)}_{P_{ij}\equiv Stress\ Production} \\
&\underbrace{+\overline{p\left(\frac{\partial u_\iota}{\partial x_j} + \frac{\partial u_j}{\partial x_\iota}\right)}}_{\emptyset_{ij}\equiv Pressure\ Strain} \underbrace{-2\mu\overline{\frac{\partial u_\iota}{\partial x_k}\frac{\partial u_j}{\partial x_k}}}_{\epsilon_{ij}\equiv Dissipation} + \rho\left(\underbrace{\overline{u_i f_j} + \overline{u_j f_i}}_{F_{ij}\equiv\text{force-coupling}}\right) + \rho\left(\underbrace{\overline{u_i g_j} + \overline{u_j g_i}}_{G_{ij}\equiv\text{torque-coupling}}\right)
\end{aligned} \tag{60}$$

Where $\tau_{ij} = \overline{u_\iota u_j}$ is the symetric Reynolds stress tensor. Dividing this tensor by two, we get the equation for the fluctuation kinetic energy, which is: $k = \frac{1}{2}\overline{u_\iota u_j}\delta_{ij}$ where δ_{ij} is the Kronecker delta. Applying this to the dissipation term, we get:

$$2\mu\overline{\frac{\partial u_\iota}{\partial x_k}\frac{\partial u_j}{\partial x_k}}\delta_{ij} = 2\mu\overline{\frac{\partial u_\iota}{\partial x_k}\frac{\partial u_\iota}{\partial x_k}} \tag{61}$$

The trace of the dissipation term in the Reynolds stress tensor is twice the homogeneous dissipation, and hence:

$$\epsilon = 0.5(\epsilon_{11} + \epsilon_{22} + \epsilon_{33}) \tag{62}$$

2.3 Transfer of Kinetic Energy

The distribution of the turbulent kinetic energy is divided into production, diffusion and dissipation, i.e. energy absorbed, redistributed and energy lost through heat due to viscous forces. The kinetic energy is produced in the mean flow and transferred from the fluctuating flow and is lost by a heat increase through the energy cascade. The interaction of motion of different scales, known as eddies, describe this energy transfer. When a fluid flows past an obstacle, the swirling and the reserve current created is known as an eddy. This term collects identifiable turbulent patterns such as velocity and pressure. We can observe the kinetic energy transfer by identifying terms in the equations of mean and fluctuating kinetic energy.

$$\frac{\partial k}{\partial t} + U_j \frac{\partial k}{\partial x_j} = -\frac{\partial}{\partial x_j}\left[\frac{1}{\rho}\overline{u_j p} + \frac{1}{2}\overline{u_\iota u_j u_k} - 2\nu\overline{u_\iota s_{\iota j}}\right] - \underbrace{\overline{u_\iota u_j} S_{ij}}_{\text{Source}} - 2\nu\overline{s_{\iota j} s_{\iota j}} \quad (63)$$

$$\frac{\partial K}{\partial t} + U_j \frac{\partial K}{\partial x_j} = -\frac{\partial}{\partial x_j}\left[\frac{1}{\rho}\overline{U_j p} + \frac{1}{2}\overline{U_\iota u_j u_k} - 2\nu\overline{U_\iota s_{\iota j}}\right] + \underbrace{\overline{u_\iota u_j} S_{ij}}_{\text{Sink}} - 2\nu\overline{S_{\iota j} S_{\iota j}} \quad (64)$$

This term, $\overline{u_\iota u_j} S_{ij}$ is repeated in both equations but with different signs. This is because this term is usually negative, so the energy is transferred from the mean flow to the fluctuations.

2.3.1 Turbulence Scales and the Energy Cascade

In 1941 [26], Kolmogorov introduced a turbulent scale, this scale is explained by having energy from larger energy containing turbulent structures that feeds smaller turbulent structures. Kolmogorov suggested that the unstable large eddies continues to break until the forces of viscosity stabilizes the eddies and energy leave the flow through molecular viscosity causing an entropy increase. This was done with the assumption of homogeneous, isotropic turbulence and high Reynolds number.

The scales of length, time and velocity are presented by l, t & u respectively where $t = l/u$. Kolmogorov micro-scales are the smallest scales in turbulent flow. At the Kolmogorov scale, viscosity dominates and the turbulent kinetic energy is dissipated into heat. They are defined by:

$$\eta = \left(\frac{v^3}{\epsilon}\right)^{1/4} \text{ Kolmogorov Length Scale} \quad (65)$$

$$\tau = \left(\frac{v}{\epsilon}\right)^{1/2} \quad \text{Kolmogorov Time Scale} \quad (66)$$

$$v = (v\epsilon)^{1/4} \text{ Kolmogorov Velocity Scale} \quad (67)$$

By introducing these variables into the Reynolds number, we get:

$$Re = \frac{1}{v}(v\epsilon)^{1/4}\left(\frac{v^3}{\epsilon}\right)^{1/4} = \frac{1}{v}\left(\frac{v\epsilon v^3}{\epsilon}\right)^{1/4} = 1 \quad (68)$$

This shows that the viscous effects are always important at these scales.

Chapter 3

Direct Numerical Simulation

There are three Computational Fluid Dynamics (CFD) methods available to solve the turbulent flow numerically. Reynolds-Average Navier-Stokes (RANS) simulation is the most conventional numerical technique where the turbulent Reynolds stress has to be modelled. This method is widely used in solving industry problems with its fast and economic characteristics but it has a non-guaranteed accuracy regarding to the results. The Large Eddy Simulation (LES) can directly compute the large scales of turbulent flow while the small scales are modelled with subgrid models. The LES can achieve a higher accuracy than the RANS. The last method is solving the Navier-Stokes equations from the first principles without any kind of modelling, this is called Direct Numerical Simulation (DNS). DNS resolves all relevant scales from the smallest dissipative Kolmogorove scale to the integral one, these results in having great details regarding the physics of turbulence. High resolution computational mesh and time step are needed to capture the smallest eddy DNS, this leads to huge consumption of memory and CPU hours.

3.1 Flow Domain and Equations

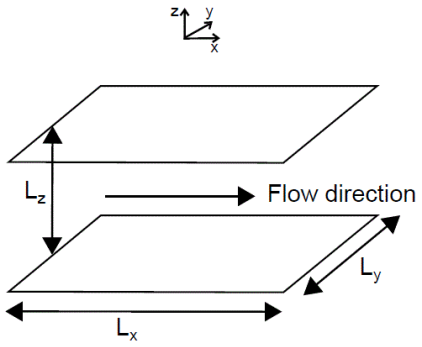

Figure 3. 1

The flow domain

Figure 3. 1 illustrates the domain solved by means of Direct Numerical Simulation in this thesis, where $L_x = 2\pi, L_y = \pi \; and \; L_z = H = 1$ represent the streamwise, spanwise and wall normal direction respectively. Solving the Navier-Stokes equations happens in their non-dimensional form indicating that the variables are scaled by their characteristic counter part. The star indicates a non-dimensional variable:

$$x^* = x/H, \quad \overrightarrow{u^*} = \vec{u}/u_\tau, \quad t^* = tu_\tau/L, \quad p^* = p/(\rho u_\tau^2) \tag{69}$$

By inserting these into Eq. (33):

$$\frac{\partial \rho u_i^* u_\tau}{\partial t^* H/u_\tau} + \frac{\partial \rho u_i^* u_\tau u_j^* u_\tau}{\partial x_j^* H} = -\frac{\partial p^* \rho u_\tau^2}{\partial x_i^* H} + \mu \frac{\partial^2 u_i^* u_\tau}{\partial x_j^* H \partial x_j^* H} + \vec{f} \quad (70)$$

Where $\vec{f} = -\frac{1}{\Delta}\sum_{i=1}^{n_p} \vec{F}$ is the force per unit volume from the particles and $\vec{f}^* = \vec{f}\, L/\rho U^2$

The point-force from an individual particle on the fluid is equal to $-\vec{F}$ based on Newton's third law as illustrated in Figure 3. *2*

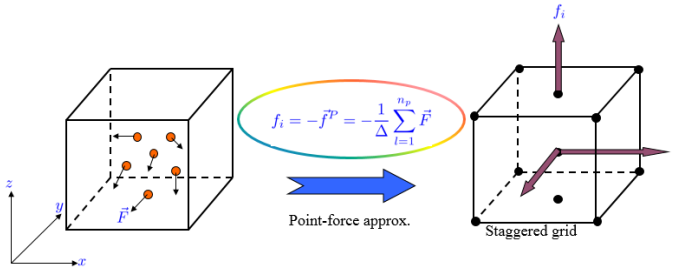

Figure 3. 2

Point particle-forces $\vec{F}$ transferred into volume force $\vec{f}$

Multiplying Eq. (70) by H/u_τ, we get:

$$\frac{\partial u_i^*}{\partial t^*} + \frac{\partial u_i^* u_j^*}{\partial x_j^*} = -\frac{\partial p^*}{\partial x_i^*} + \frac{H}{\rho u_\tau^2}\frac{\mu u_\tau}{H^2}\frac{\partial^2 u_i^*}{\partial x_j^* \partial x_j^*} + \frac{H}{u_\tau}\vec{f} \quad (71)$$

Having $\frac{H}{\rho u_\tau^2}\frac{\mu u_\tau}{H^2} = \frac{1}{Re_\tau}$, then Eq. (71) would look like this [29]:

$$\frac{\partial u_i^*}{\partial t^*} + \frac{\partial u_i^* u_j^*}{\partial x_j^*} = -\frac{\partial p^*}{\partial x_i^*} + \frac{1}{Re_\tau}\frac{\partial^2 u_i^*}{\partial x_j^* \partial x_j^*} + \vec{f}^* \quad (72)$$

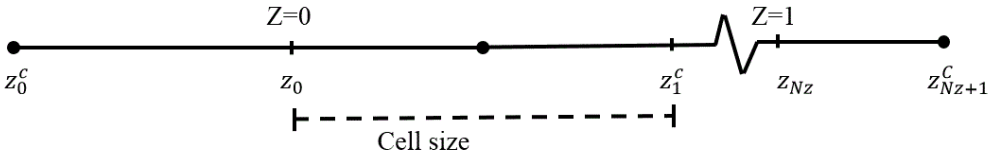

Figure 3. 3

Discretization domain in z-direction.

$u_\tau = \sqrt{\tau_w/\rho}$ is called the friction velocity where it relates the wall shear stress to a velocity. Eq. (72) presents the non-dimensional form of Navier-Stokes solved in the DNS code where $Re_\tau = 360$, the constant pressure gradient $-dp^*/dx^* = 2$, no-slip condition at the wall and periodic boundary conditions at the remaining directions.

3.2 Discretization

In this thesis, pseudospectral method is applied because of the homogeneous turbulent flow in the stream-wise and span-wise directions. The Navier-Stokes equations are solved using Fourier

transforms in the homogeneous directions; while a second order staggered finite difference method is applied in wall normal direction.

We discretize the domain by a uniform grid in stream-wise and span-wise directions by having the cell sizes as such:

$\Delta x = 2\pi/N_x \; and \; \Delta y = \pi/N_y$, where N_x and N_y are the number of grid points. As shown in Figure 3. 3, the cell size is stretched by a harmonic continuous function yielding finer grid resolution near the walls in the wall normal direction.

$$\vec{z}(\vec{k}, s) = \frac{1}{2}\frac{arctan\left(s\left(\vec{k}-\frac{1}{2}\right)\right)}{arctan\left(s\frac{1}{2}\right)} + \frac{1}{2} \tag{73}$$

Where s is a stretching factor and $\vec{k} = [0,1,2, \ldots\ldots, N_z]/N_z$, meaning that the cell size in the wall normal direction is given by:

$$\Delta z_i = z(k_i) - z(k_i - 1) \qquad \text{for} \qquad i = 1,2,3, \ldots\ldots, N_z \tag{74}$$

Stream-wise and span-wise velocities together with the pressure field are calculated at the cell center, which we define as:

$$z_i^C = \frac{1}{2}(z_i + z_{i-1}) \qquad \text{for} \qquad i = 1,2,3, \ldots\ldots, N_z \tag{75}$$

The wall normal velocities are calculated at the face of the cell.

Spatial derivatives

In the wall normal direction, we choose a second-order difference scheme while giving a first-order accuracy on a non-uniform grid. All derivatives of cell centered properties are defined at the cell faces and opposite. This means:

$$\frac{d}{dz}u_i^F = \frac{u_{i+1}^C - u_i^C}{z_{i+1}^C - z_i^C} \qquad \frac{d}{dz}u_i^C = \frac{u_i^F - u_{i-1}^F}{z_i^F - z_{i-1}^F} \tag{76}$$

The derivation of second-derivatives is successive use of the above equations. If a property saved at a cell face is needed at the cell center, the interpolation scheme is simply the arithmetic mean of averaging.

$$u_i^F = \frac{1}{2}\left(u_{i+1}^C + u_i^C\right) \qquad u_i^C = \frac{1}{2}(u_i^F + u_{i-1}^F) \tag{77}$$

The derivatives in the homogeneous directions are calculated by the means of Fourier transformations. The variables are transformed from physical space and into the spectral space where the calculations of derivatives are easier and much more accurate. Consider the velocity vector $\vec{u}$

$$\vec{u}(\vec{x}, t) = \sum_k \vec{\hat{u}}(t) e^{i\vec{k}\vec{x}} \tag{78}$$

Where $\vec{x} = [x, y, z]$ is the position vector in physical space and $\vec{k} = \left[k_x, k_y, z, t\right]$ is the wave number vector in spectral space. By having i as the imaginary number, the derivation of the

transformed variable is done by multiplying with $i\vec{k}$. Therefore, we get the first and second derivative of $\vec{u}$ in the stream-wise direction as such:

$$\frac{d}{dx}\vec{u}(\vec{x},t) = \sum_k \vec{\hat{u}}_k(t) i\vec{k}_x e^{i\vec{k}\vec{x}} \qquad \frac{d^2}{dx^2}\vec{u}(\vec{x},t) = -\sum_k \vec{\hat{u}}_k(t)\vec{k}_x^2 e^{i\vec{k}\vec{x}} \tag{79}$$

By solving the system of equations and calculating the derivatives, the terms are back to the physical space.

For time integration, an explicit second-order accurate Adams-Bashforth scheme is used [27].

$$y_{n+2} = y_{n+1} + h\left(\frac{3}{2}f(t_{n+1}, y_{n+1}) - \frac{1}{2}f(t_n, y_n)\right) \tag{80}$$

Applying Eq. (78) to Navier-Stokes [28]:

$$\frac{\vec{u}^{n+1} - \vec{u}^n}{\Delta t} = \frac{3}{2}T(\vec{u}^n) - \frac{1}{2}T(\vec{u}^{n-1}) - \Delta p^{n+1} \tag{81}$$

Where $T(\vec{u}^n) = -(\vec{u}^n.\nabla)\vec{u}^n + Re_*^{-1}\nabla^2\vec{u}^n$. The only unknowns are $\vec{u}^{n+1}$ *and* p^{n+1}.

Therefore, we solve Eq. (81) without the pressure term, yielding a temporary value for the velocity $\vec{u}_*$.

$$\frac{\vec{u}_* - \vec{u}^n}{\Delta t} = \frac{3}{2}T(\vec{u}^n) - \frac{1}{2}T(\vec{u}^{n-1}) \tag{82}$$

As explained before, the upper star index represents a non-dimensional value where the lower index star indicates an intermediate value. By subtracting Eq. (82) from Eq. (81), we get:

$$\vec{u}^{n+1} - \vec{u}_* = -\Delta t\nabla p^{n+1} \tag{83}$$

By considering the divergence of Eq. (81):

$$\nabla.\vec{u}^{n+1} - \nabla.\vec{u}_* = \Delta t\nabla^2 p^{n+1} \tag{84}$$

To satisfy the continuity Eq., $\nabla.\vec{u}^{n+1}$ must be equal to zero and this reaches to a Poisson equation for the pressure presented as:

$$\nabla^2 p^{n+1} = \frac{\nabla.\vec{u}_*}{\Delta t} \tag{85}$$

This equation is solved by using fast Fourier transforms, and then used to find the velocity at the new time step by using Eq. (84).

Chapter 4

Results

The Downlflow statistics of the velocity field for both fluid and bubbles are presented here. In 1987, [30] Kim *et al.* performed a DNS of the turbulent channel flow and is still regarded as a standard reference for wall-bounded turbulent flow until now. The results in this thesis will be subject to comparison with Kim *et al.* as well. Three different cases are studied related to three different bubbles' diameter, $d = 110, 220\ and\ 330\ \mu m$.

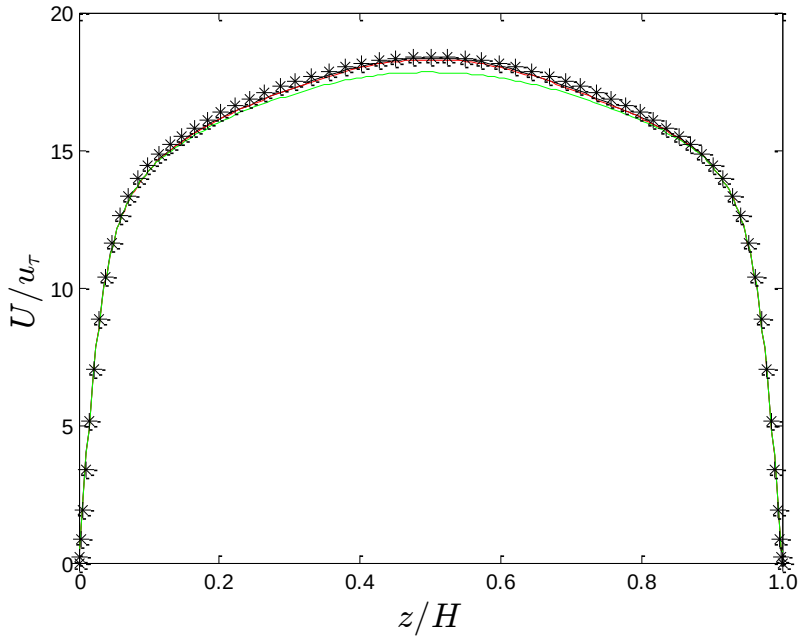

Figure 4. 1

Mean velocity profile for three different bubbles diameter (––d=330μm, ––d=220μm while ––d=110). ((∗) Denotes DNS data from Kim et al.) Compared with data from Kim et al.

4.1 Mean flow properties

Figure 4. 1 illustrates the differences in the mean velocity profile as the diameter of the bubble differs. The mean velocity profile moves towards a greater maximum and "flatter" curvature near the channel center, i.e. dU/dz moves closer to zero in this region. As proven by D. Molin [6], the velocity is reduced in a downflow stream due to the effect of the lift force presented by the bubbles. This is confirmed in our results where the velocity decreases gradually as the bubbles' diameter increase. This is due to the increase in the lift force (buoyancy) as the bubble diameter increase.

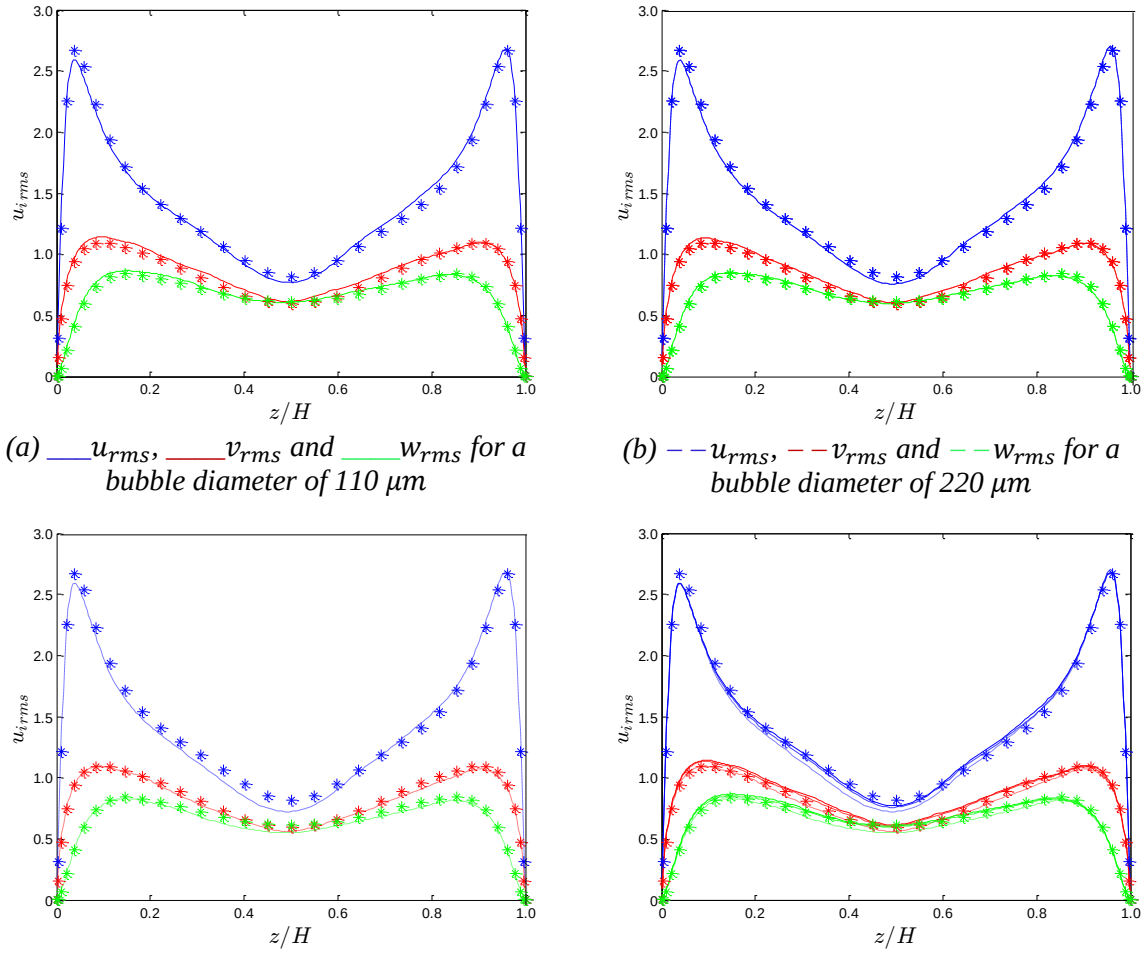

(a) ___u_{rms}, _____v_{rms} and _____w_{rms} for a bubble diameter of 110 μm

(b) – –u_{rms}, – –v_{rms} and – –w_{rms} for a bubble diameter of 220 μm

(c) ..... u_{rms}, ...v_{rms} and .....w_{rms} for a bubble diameter of 330 μm

(d) The three cases all together

Figure 4. 2

Root mean squared of velocity components for the different bubbles diameter compared with data from Kim et al [30], normalized with u_τ.

4.1.1 Turbulent Intensities

Figure 4. 2 illustrates the velocity fluctuations, or the turbulent intensities in the streamwise u_{rms}, spanwise v_{rms} and the wall normal direction w_{rms}, which are symmetric about the centerline of all grids. Figures 4.2 (a, b and c) presents the velocity fluctuations for the three different bubble diameter of 110, 220 and 330 μm respectively. Here, we can see that for all the cases, u, v and w fluctuations are reduced as the bubble diameter increases compared with Kim et al. This is clear by a slight increase with the under prediction at the center as the bubble diameter increases in the streamwise component. Case (d) combines all the diameters and provides us with a clear view how the fluctuation decreases as the diameter increases. Yet we can see that the fluctuation for both cases (*a and b)* are almost the same, the main difference is compared with case (*c*) where (*d=330μm).* This will have an impact on the Reynolds stress budget, which will be presented in 4.2.

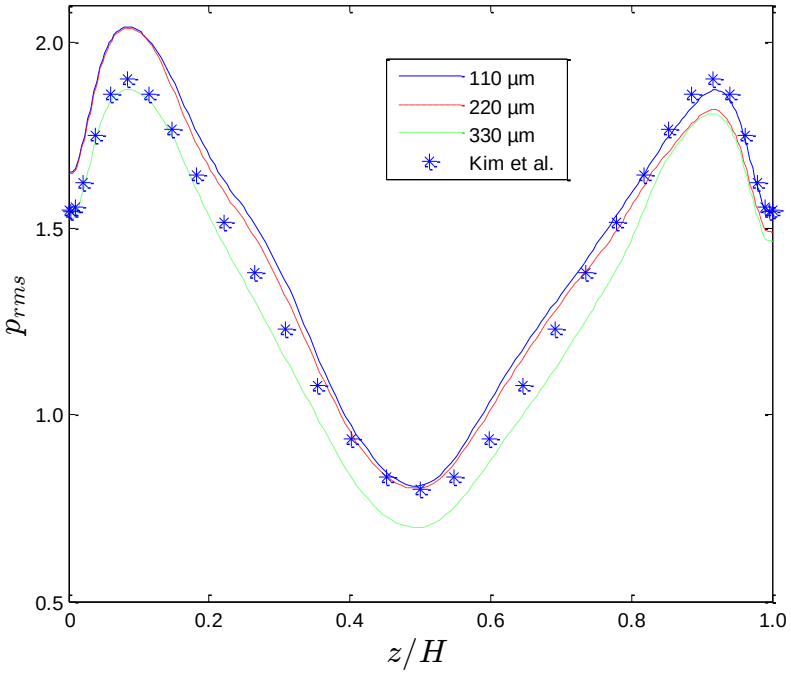

Figure 4. 3

Root-mean-square pressure fluctuations normalized by the wall shear velocity $p_{rms}/\rho u_\tau^2$.

Figure 4. 3 shows the profile of root-mean-square (r.m.s.) pressure normalized by the wall shear velocity, $p_{rms}/\rho u_\tau^2$. We can see that in both cases for $d = 110\ and\ 220\mu m$, the results under predicts the values near the wall while for $d = 330\mu m$,while they over predicts the value at the center. This can be explained due to the lack of accumulation build-up near the wall and the increase in the lift effect presented by the bubbles to the fluid that increases as the bubble diameter increases. In addition, the Kolmogorov length and time scales are 5 to 10 times larger at the center than at the wall, which has a larger effect on the pressure especially as the particle diameter increases.

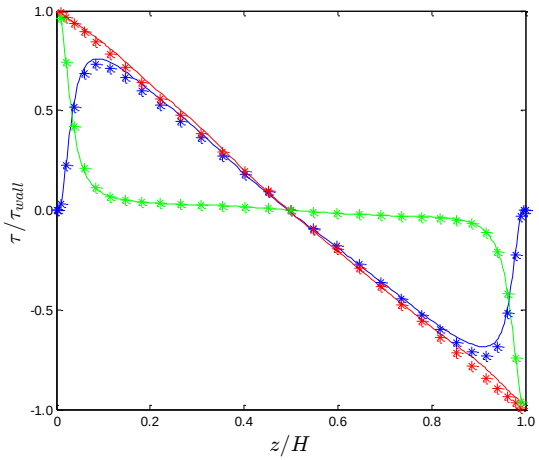

(a) Shear forces for $(d = 110\mu m)$

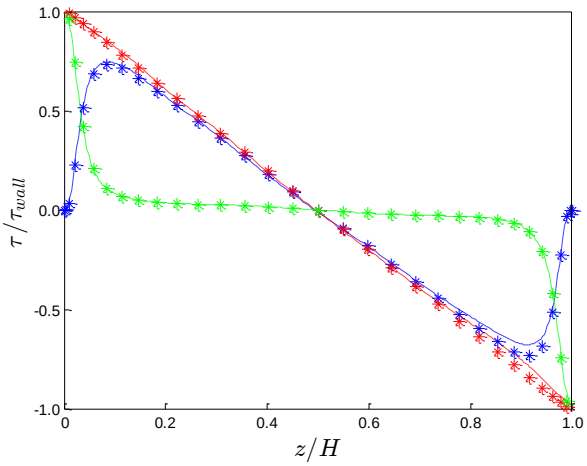

(b) Shear forces for $(d = 220\mu m)$

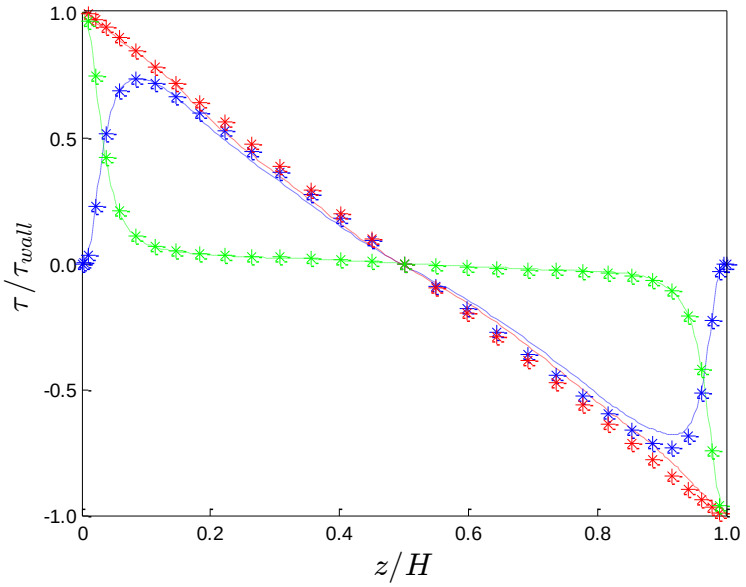

Figure 4. 4

(c) Shear forces for $(d = 330\mu m)$ *where blue line is* uw/τ_w, *red line is* $(vdu/dz - uw)/\tau_w$ *and green line is* $(vdu/dz)/\tau_w$.

4.1.2 Reynolds Shear stress

Figure 4. 4 shows the Reynolds shear stress in the flow. In all the cases of the three different bubbles' diameter of 110, 220 and $330\mu m$, we get the exact value compared with the data provided by Kim et al. as denoted by the star $(*)$.

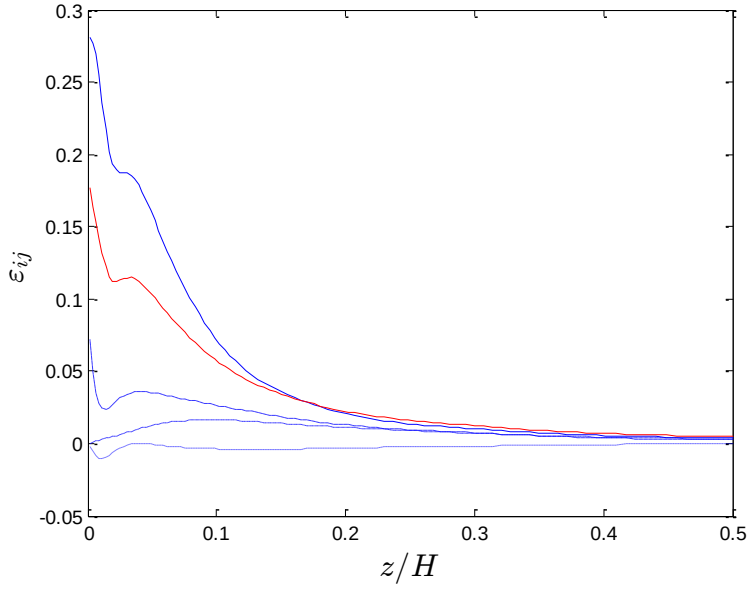

Figure 4. 5 $-\epsilon_{11}, --\ \epsilon_{22}, -.\epsilon_{33}, \ldots\ \epsilon_{13}$ *and* $-\epsilon$ *for bubbles' diameter of* $110\mu m$

4.1.3 Dissipation

Figure 4. 5 shows the turbulent dissipation for case (*d=110μm*), other cases (*d=220 and 330 μm*) shows to be the same. As expected, due to largest derivatives of the velocity fluctuation, ϵ_{11} shows to be the dominating term then followed by ϵ_{22}, and then ϵ_{33}.

$\epsilon = 0.5(\epsilon_{11} + \epsilon_{22} + \epsilon_{33})$ (Presented by the red line).

There are no data presented by Kim to be compared to but as explained, the results are suitable compared with the physics of dissipation.

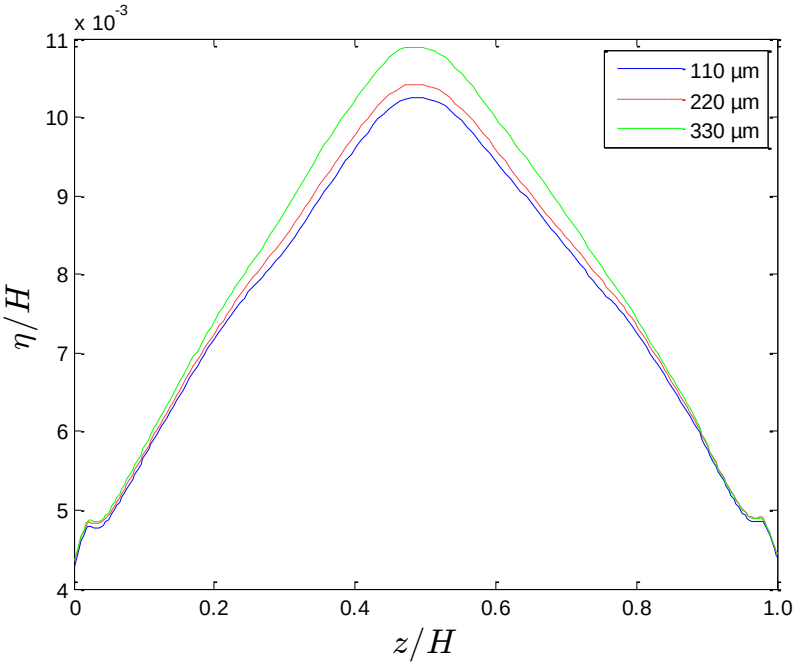

Figure 4. 6 (Kolmogorov length scale)

4.1.4 Kolmogorov Length Scale

In Figure 4. 6, the Kolmogorov length scale η/H is presented for the three cases. Since the length scale is presented as a function of the dissipation as shown in Eq. (65), we expect an opposite behavior since $\eta = \left(\frac{\nu^3}{\epsilon}\right)^{1/4}$.

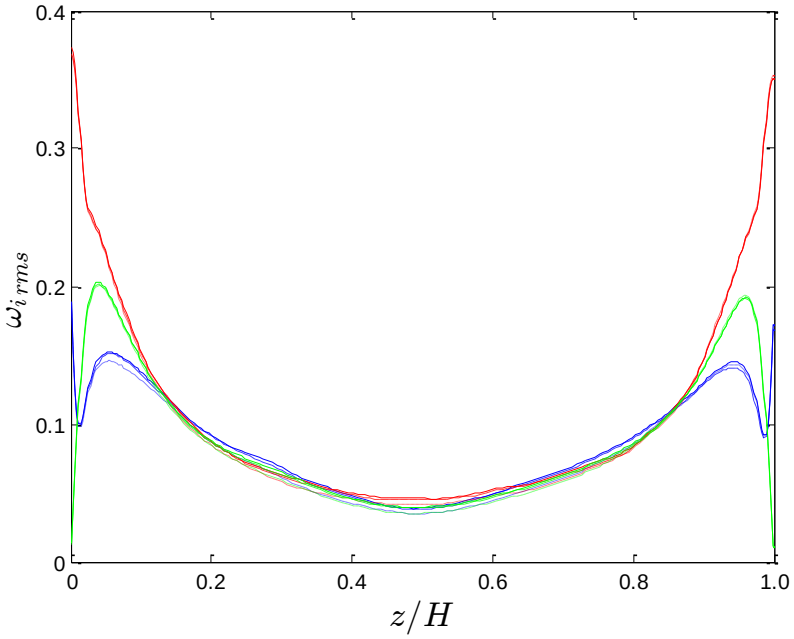

Figure 4. 7 Root-mean-square vorticity fluctuations normalized by the mean shear in global coordinates. (For the three cases)

4.1.5 Vorticity

In Figure 4. 7, we can see the stream wise vorticity fluctuations normalized by the mean shear at the wall ($w_i v/u_\tau^2$). For all the three cases, the results agree with data from Kim et al. It is worthy explaining the vorticity presented as:

$$\begin{aligned} w_i &= \epsilon_{ijk}\frac{\partial u_k}{\partial x_j} \\ w_x &= \frac{\partial w}{\partial y} - \frac{\partial v}{\partial z} \\ w_y &= \frac{\partial u}{\partial z} - \frac{\partial w}{\partial x} \\ w_z &= \frac{\partial v}{\partial x} - \frac{\partial u}{\partial y} \end{aligned} \tag{86}$$

4.1.6 Skewness and Flatness

Figure 4. 8 illustrates the Skewness that is defined as a measure of asymmetry of a function with respect to the origin. Skewness can take on both positive and negative values, and that observed in turbulence experiments is usually negative. Just as will be the case for flatness that will be explained in the next paragraph. The S$(u_i)$is presented *as* u_i, v_i *and* w_i and compared with Kim at al. it is clear that results agree with Kim et al. It is worthy presenting the equation presenting the Skewness as:

$$S_i = \frac{\overline{u_i u_i u_i}}{(\overline{u_i u_i})^{3/2}}$$

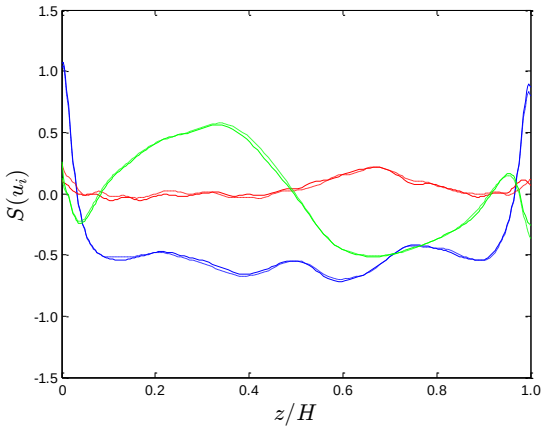

Figure 4. 8

Higher-order component of the velocity fluctuation u_i. Skewness $S(u_i)$ where —u_i, —v_i and —w_i.

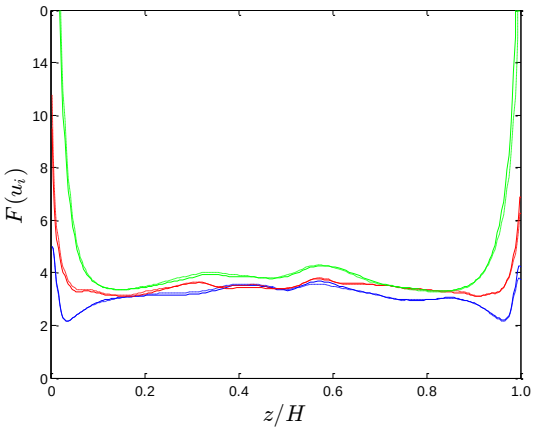

Figure 4. 9

Flatness $F(u_i)$ where —u_i, —v_i and —w_i.

Figure 4. 9 presents Flatness that requires an equation for formal definition. Here we simply note that it represents the deviation from Gaussian in the sense that functions having large flatness values are more sharply peaked than are Gaussian distributions, and conversely. Flatness (sometimes called "kurtosis") is always greater than zero unlike Skewness that can be less than zero. The results presented agree Kim et al. and the equation for the Flatness is as:

$$F_i = \frac{\overline{u_i u_i u_i u_i}}{(\overline{u_i u_i})^2}$$

4.2 Reynolds-stress budgets

The budgets of the individual components of the Reynolds stress tensor provide insight into the interaction between the large-scale turbulence and the mean flow. The budgets of the three diagonal components and the only off-diagonal Reynolds stress component are shown in *Figure 4. 10* (*d=110μm).* This has been compared to Barri [32] and showed perfect match.

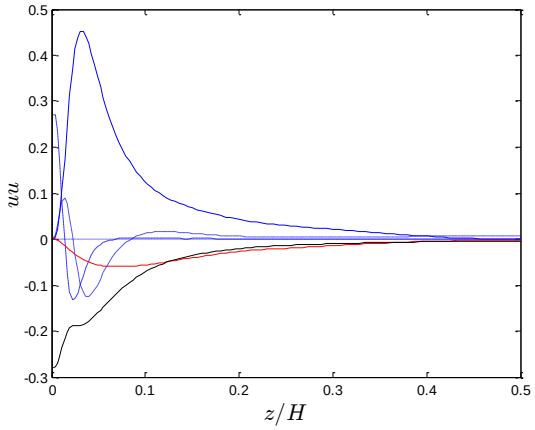

(a)uu

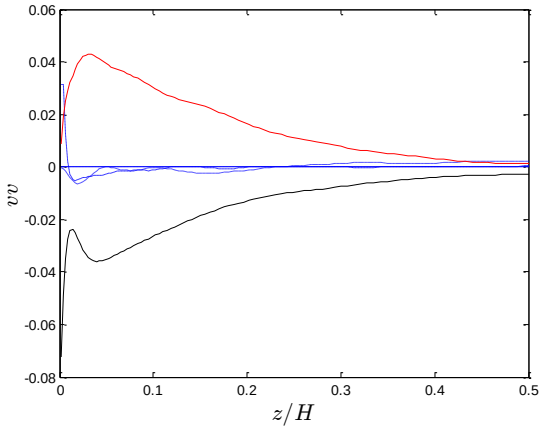

(b) vv

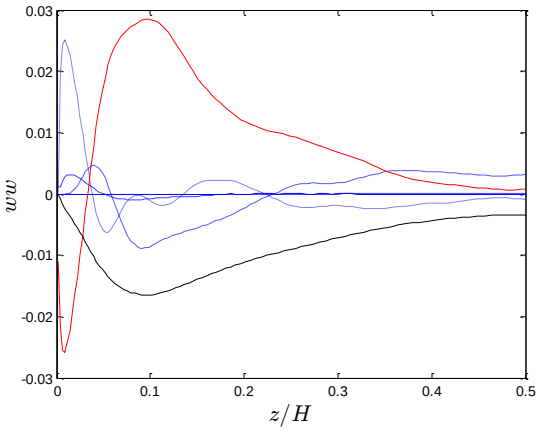

(c) ww

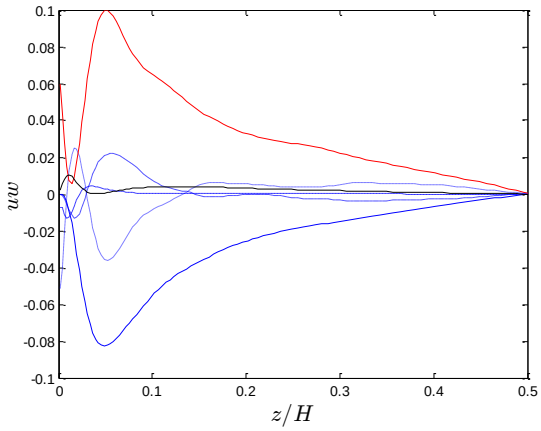

(d)uw

Figure 4. 10 budgets of the individual components of the Reynolds stress tensor.

Where $-(\varnothing_{ij})$ is the Pressure strain distribution. $-(\epsilon_{ij})$ is the viscous energy dissipation. $-(P_{ij})$ is the Production due to mean shear. $--(D_{ij}^{V})$ is the viscous diffusion. $-\cdot-(D_{ij}^{T})$ is the turbulent diffusion due to velocity fluctuation. $\cdots(D_{ij}^{P})$ is the turbulent diffusion due to pressure fluctuation. See Appendix.

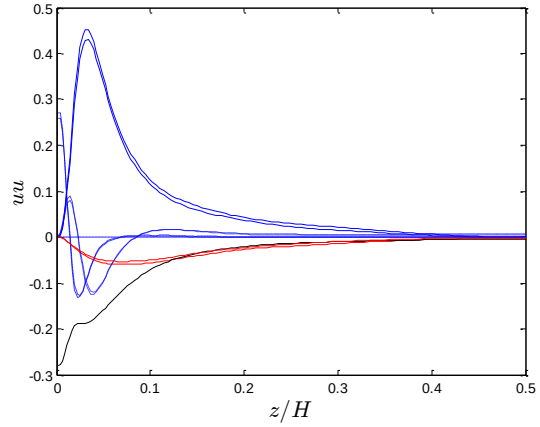

(a) comparison between uu (for d=330μm and for d=110μm)

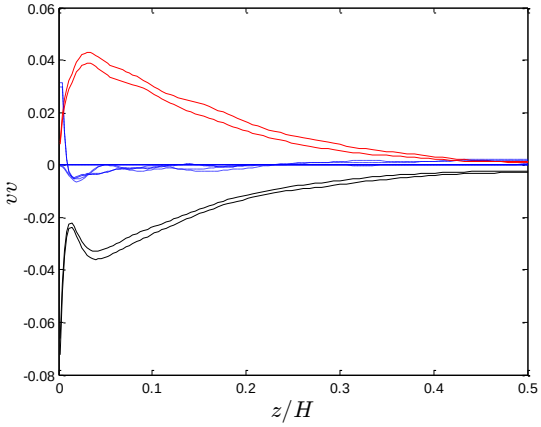

(b) comparison between vv (for d=110μm and d=330μm)

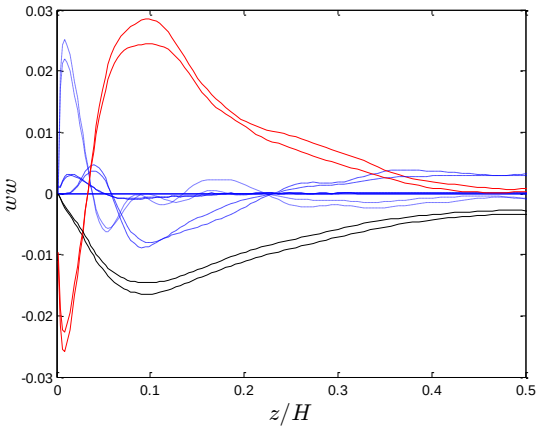

(c) comparison between ww (for d=110μm and d=330μm)

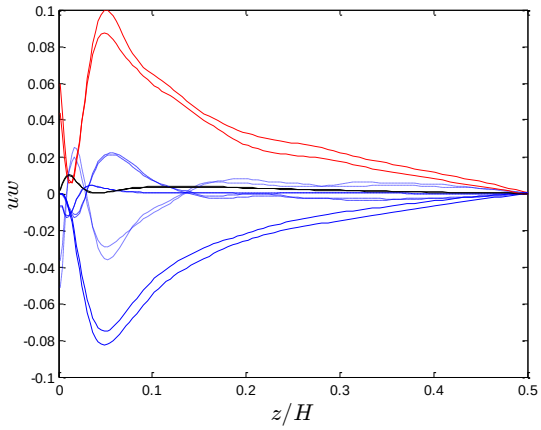

(d) comparison between uw (for d=110μm and d=330μm)

Figure 4. 11

Figure 4. 11 illustrates the difference in results we get when comparing the Raynolds-stress budgets for both *d=110µm and d=330µm*. Analyzing (a), no major differences are observed between the two cases other than a slight decrease in the production term for *d=330µm*. For both (b and c), a decrease in both the pressure distribution and viscous dissipation is observed as the diameter increases. As for part (d), the pressure distribution and the production term tend to decrease as the diameter of the bubble increases. This is very convenient since both the production and the diffusion terms are dependent on the Reynolds stress term as shown in Eq. (60).

4.2 Particle statistics

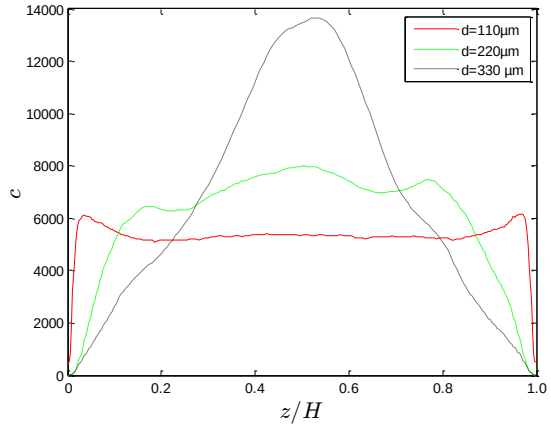

(a) Bubbles concentration along the channel for all three cases

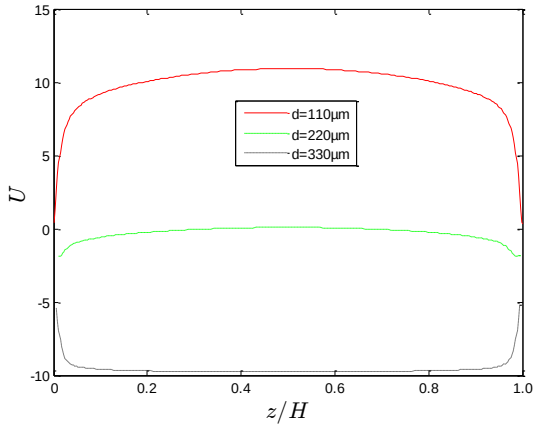

(b) Particle average velocity profile for the three cases

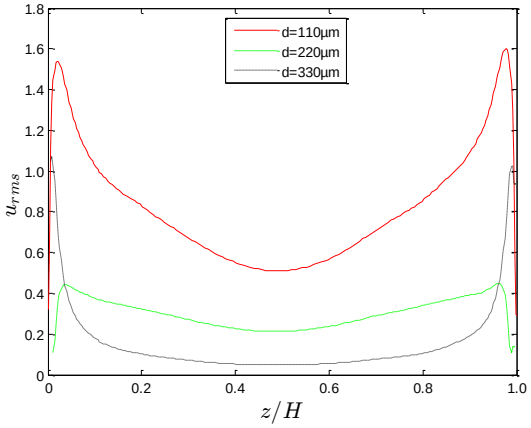

(c) u_{rms} for the three cases

Figure 4. 12 u_{rms} for the Particles.

Figure 4. 12 shows three different results for the particle statistics, part (a) provides us with the concentration of the particles in the channel and we can clearly see that as the diameter increases, the concentration of the particles increases in the center and decreases at the wall. On the other hand, the concentration decreases at the center to reach constant as the particle diameter decreases. Part (b) shows the average velocity profile of the bubble phase, when comparing with the average velocity profile of the liquid phase, presented by Figure 4. 1, we can see that the bubble phase moves slower than the liquid phase due to the buoyancy pulling

and the liquid without bubbles flows slightly faster than the liquid laden with bubbles in the downflow. It is clear that the bigger the bubble diameter, the more effect it has on the fluid phase. And this agrees with Mazzitelli et al as he considered that microbubbles accumulating in down-flow regions locally transfer momentum upwards, and therefore, the microbubble addition reduces the vertical velocity fluctuation intensity and the turbulent kinetic energy.

Part c shows the u_{rms} for the three cases and as we can see, as the bubble diameter increases, u_{rms} decreases.

4.3 Instantaneous particles distribution

In Figure 4. 13, we can see the instantaneous distribution of bubbles when the bubble motions reach a statistically steady state. We can also see how the bubbles (*d=110µm)* do not accumulate near the walls and the concentration is mainly constant through the channel apart from the wall. As for Figure 4. 14, the particle turbulence is presented.

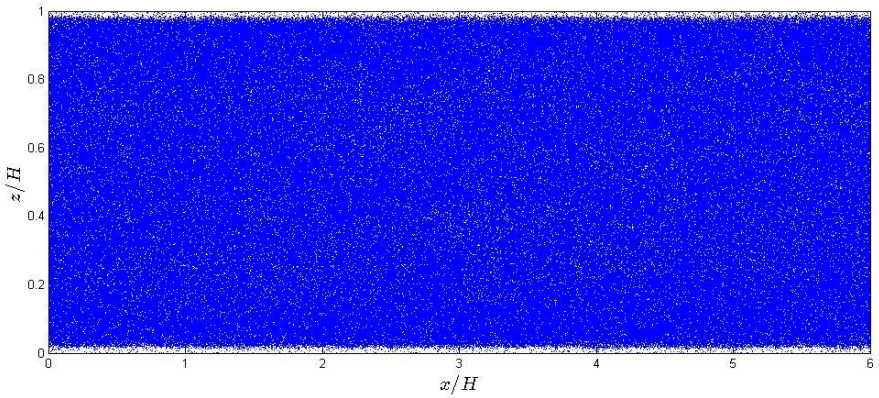

Figure 4. 13 instantaneous distribution of bubbles in Channel.(d=110µm)

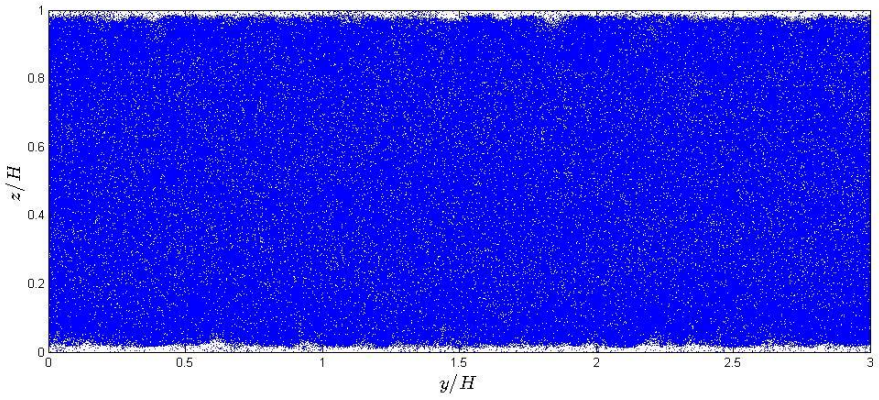

Figure 4. 14 Particle turbulence (d=110µm)

Figure 4. 15, presents as well the instantaneous distribution of bubbles of diameter *d=220µm* and it is obvious when compared with Figure 4. 13, how the bubbles' concentration increases at the center. This is a reflection for the concentration plot that was presented in Figure 4. 12 (a). In Figure 4. 16, we see how the turbulence increases as the particle diameter increases.

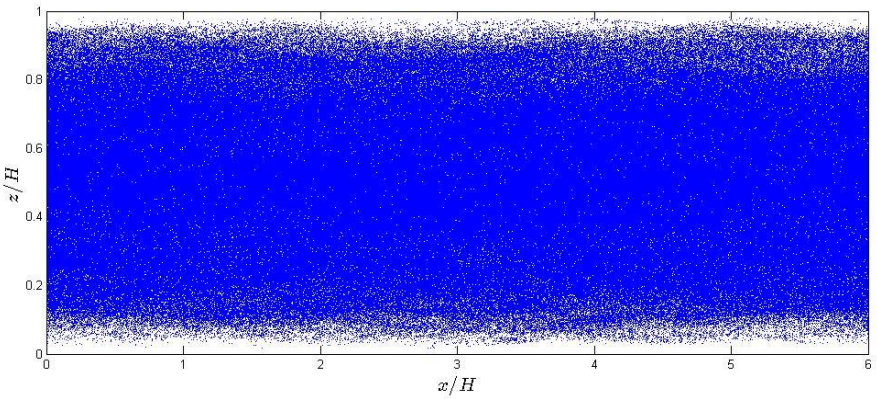

Figure 4. 15 instantaneous distribution of bubbles in Channel.(d=220µm)

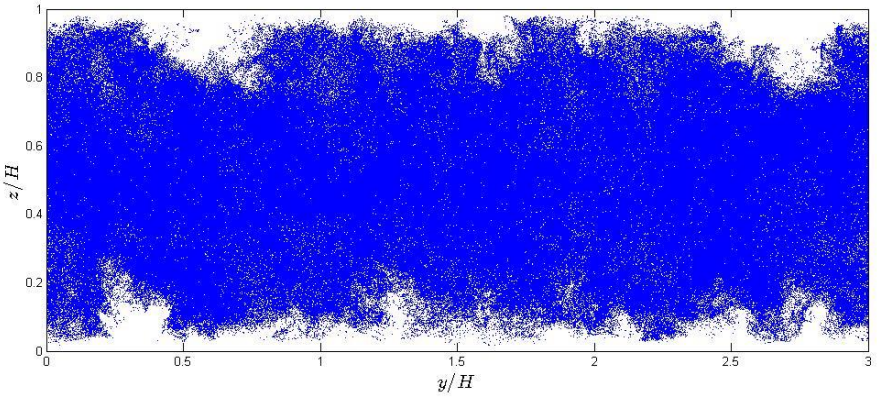

Figure 4. 16 Particle turbulence (d=220µm)

Finally, Figure 4. 17 presents as well the instantaneous distribution of bubbles of diameter *d=330µm* where the concentration of the particles increases obviously at the center of the channel. At the same time, Figure 4. 18 shows how the turbulence increases as well as the diameter of the particle increases which is obvious since the Reynolds number depends on the particle diameter which influence the turbulence as well.

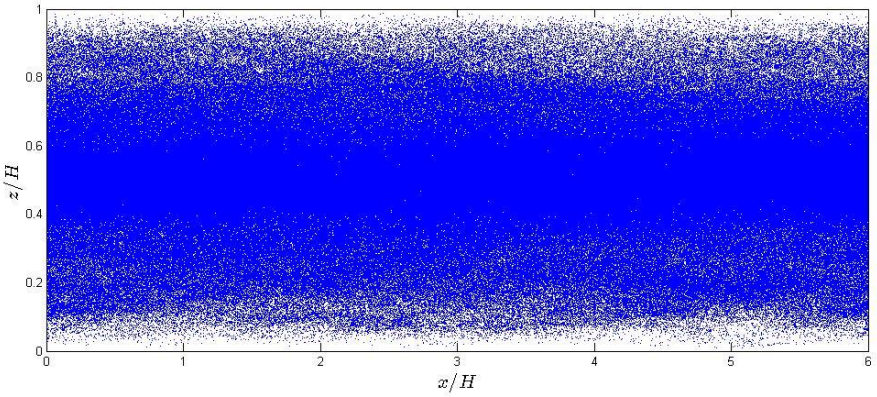

Figure 4. 17 instantaneous distribution of bubbles in channel (d=330µm)

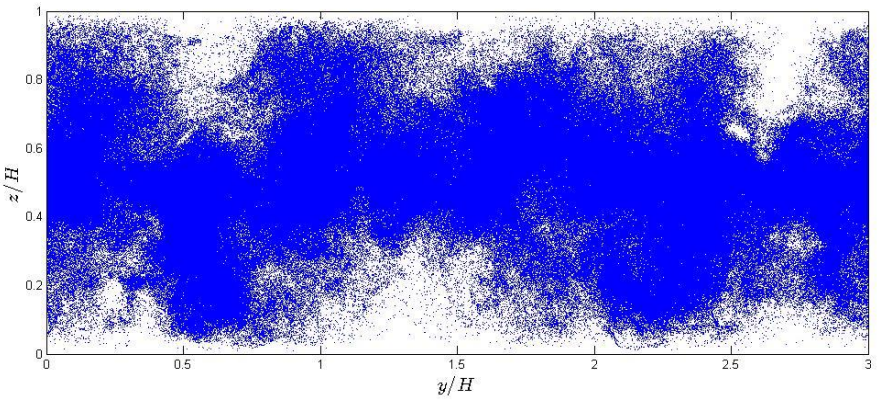

Figure 4. 18 Particle turbulence (d=330μm)

Chapter 5

5.1 Conclusions

In this Thesis, we have presented results from direct numerical simulations (DNS) of turbulent microbubble dispersion in vertical channel flow for downflow conditions. Bubbles interact with the surrounding fluid by exchanging momentum. Several important conclusions can be summarized as follows.

(1) Bubbles move rapidly away from the wall under the aid of the shear lift force and the turbulence, which leads to the present distribution pattern.
(2) The bubble injection leads to the liquid velocity decrease by the bubble pulling, slightly intensifies the liquid turbulence as the particles increase in diameter. In the channel central region, the particles concentration increases as well as the diameter increases.
(3) The bubbles' increase in diameter reduces the liquid-phase Reynolds stress

5.2 Future recommendation

It is very well recommended to study the same case but in the upflow direction where the buoyancy would play an opposite effect on the fluid velocity and compare it to this case. This would give us a better understanding regarding the lift force and its influence on the overall fluid.

It is worthy to mention that this work was discussed, planned and executed in a period of two months only, and proudly completed.

Bibliography

[1] Lockhart, R. W., and Martinelli, R. C., 1949, "Proposed Correlation of Data for Isothermal Two Phase Flow, Two Component Flow in Pipes," Chem. Eng. Prog., 45, pp. 39–48.

[2] http://www.drbratland.com/PipeFlow2/chapter1.html

[3] A. Serizawa and I. Kataoka, "Turbulence suppression in bubbly two-phase flow," *Nuclear Engineering and Design*, vol. 122, no. 1–3, pp. 1–16, 1990.

[4] H. Kato, T. Iwashina, M. Miyanaga, and H. Yamaguchi, "Effect of microbubbles on the structure of turbulence in a turbulent boundary layer," *Journal of Marine Science and Technology*, vol. 4, no. 4, pp. 155–162, 2000.

[5] S. So, H. Morikita, S. Takagi, and Y. Matsumoto, "Laser Doppler velocimetry measurement of turbulent bubbly channel flow," *Experiments in Fluids*, vol. 33, no. 1, pp. 135–142, 2002.

[6] D. Molin, C. Marchioli, and A. Soldati, "Turbulence modulation and microbubble dynamics in vertical channel flow," *International Journal of Multiphase Flow*, vol. 42, no. 6, pp. 80–95, 2012.

[7] T. Kawamura and Y. Kodama, "Numerical simulation method to resolve interactions between bubbles and turbulence," *International Journal of Heat and Fluid Flow*, vol. 23, no. 5, pp. 627–638, 2002.

[8] I. M. Mazzitelli, D. Lohse, and F. Toschi, "The effect of microbubbles on developed turbulence," *Physics of Fluids*, vol. 15, no. 1, pp. L5–L8, 2003.

[9] A. Ferrante and S. Elghobashi, "On the physical mechanisms of drag reduction in a spatially developing turbulent boundary layer laden with microbubbles," *Journal of Fluid Mechanics*, no. 503, pp. 345–355, 2004.

[10] J. C. Lu and G. Tryggvason, "Effect of bubble deformability in turbulent bubbly upflow in a vertical channel," *Physics of Fluids*, vol. 20, no. 4, Article ID 040701, 2008.

[11] R. Clift, J.R. Grace, M.E. Weber "*Bubbles, Drops and Particles*" Academic Press, New York (1978)

[12] A. B. Basset, "*Triatise on Hydrodynamics" (Deighton Bell, London, 1888)*, Vol. 2, Chap. 22, pp.825-297.

[13] J. Boussinesq, "*Theorie Analytique de la Chaleur",* (L'Ecole Polytechnique, Paris, 1903), Vol. 2, p. 224.

[14] C. W. Oseen, "*Hydrodynamik",* (Leipzig, 1927), p. 132.

[15] C. M. Tchen, Ph.D thesis, Delft, Martinus Nijhoff, The Hague, 1947

[16] S. Corrsin and J. Lumley, Appl. Sci. Res. A 6, 114 (1956).

[17] Y. A. Buevich, Fluid Dynam. 1, 119 (1966)

[18] J. J. Riley, Ph.D. Thesis, The Johns Hopkins University, Baltimore, Maryland, 1971.

[19] M. R. Maxey, J. J. Riley, 1983. "*Equation of motion for a small grid sphere in a nonuniform flow".* Physics of Fluids 26 (4), p. 883-889.

[20] V.L. Schiller, A. Naumann, 1933. Über die grundlegenden Berechnungen bei der Schwerkraftaufbereitung. Zeitschrift des Vereines Deutscher Ingenieure 77 (12), p. 318–320.

[21] E. E. Michaelides, 2003. "*Hydrodynamic force and heat/mass transfer from particles, bubbles, and drops"*—The Freeman Schoolar Lecture. Journal
Of Fluids Engineering 125, p. 209–238.

[22] D. Legendre and J. Magnaudet, (1998), "*The lift force on a spherical bubble in a viscous linear shear flow*", J. Fluid Mech., 368, p. 81-126.

[23] L. Schiller, Z. Naumann, 1935. Z Ver. Deutsh. Ing. 77, 318.

[24] T.G. Leighton, "*Derivation of the Rayleigh–Plesset Equation in Terms of Volume*", ISVR Technical Report No. 308, 2007

[25] S. Corrsin. Interpretation of viscous terms in the turbulent energy equation. J. Aeronaut. Sci, 12:853{854, 1953.

[26] A. Kolmogorov. The local structure of turbulence in incompressible viscous fluid for very large Reynolds' numbers. In Akademiia Nauk SSSR Doklady, 30, p 301-305, 1941.

[27] E. Hairer, S. Nørsett, and G.Wanner. *Solving ordinary differential equations: Nonstiff problems*, volume 1. Springer Verlag, 1993.

[28] P. Mortensen. *Particle dynamics in wall-bounded turbulence*. Doctoral Thesis, NTNU, 2007.

[29] L. H. Zhao Ph.D. thesis, *Particles in wall turbulence*. NTNU, 2012.

[30] J. Kim, P. Moin, and R. Moser. "*Turbulence statistics in fully developed channel flow at low Reynolds number"*. Journal of Fluid Mechanics, 177(1):133-166, 1987.

[31] M. Barri, H. I. Andersson, "*Turbulent flow in a sudden-expansion channel. Part I: Effect of anti-cyclonic system rotation".* Journal of Fluid Mechanics, 665, 382-417. (2010)

[32] M. Barri, H. I. Andersson, "*Computer experiments on rapidly rotating plane Couette flow" (2009)*

Appendix

$$P_{ij} = -\overline{u_i u_k}\frac{\partial U_j}{\partial x_k} - \overline{u_j u_k}\frac{\partial U_i}{\partial x_k} \tag{A1}$$

$$D_{ij} = D_{ij}^T + D_{ij}^P + D_{ij}^V \tag{A2}$$

$$\emptyset_{ij} = \overline{\frac{p}{\rho}\left(\frac{\partial u_i}{\partial x_j} - \frac{\partial u_j}{\partial x_i}\right)} \tag{A3}$$

$$\epsilon_{ij} = 2v\overline{\frac{\partial u_\iota}{\partial x_k}\frac{\partial u_\jmath}{\partial x_k}} \tag{A4}$$

The different part of diffusion are given by:

$$D_{ij}^T = \frac{\partial}{\partial x_k}\left(\overline{u_i u_j u_k}\right) \tag{A5}$$

$$D_{ij}^P = -\frac{1}{\rho}\frac{\partial}{\partial x_k}\left(\overline{pu_i}\delta_{jk} + \overline{pu_j}\delta_{ik}\right) \tag{A6}$$

$$D_{ij}^V = v\left(\frac{\partial^2 \overline{u_i u_j}}{\partial x_k \partial x_k}\right) \tag{A7}$$

Where $i, j\ and\ k = 1,2,3$.

ϵ_{ij} is the permutation or Levi-Civita tensor.
D_{ij}^T is the turbulent diffusion due to velocity fluctuation.
D_{ij}^P is the turbulent diffusion due to pressure fluctuation.
D_{ij}^V is the viscous diffusion.